



Petrochronology and hygrochronology of tectono-metamorphic events

Valérie Bosse, Igor Villa

► To cite this version:

Valérie Bosse, Igor Villa. Petrochronology and hygrochronology of tectono-metamorphic events. Gondwana Research, 2019, 71, pp.76-90. 10.1016/j.j.gr.2018.12.014 . hal-02079961

HAL Id: hal-02079961

<https://uca.hal.science/hal-02079961>

Submitted on 18 Nov 2020

HAL is a multi-disciplinary open access archive for the deposit and dissemination of scientific research documents, whether they are published or not. The documents may come from teaching and research institutions in France or abroad, or from public or private research centers.

L'archive ouverte pluridisciplinaire **HAL**, est destinée au dépôt et à la diffusion de documents scientifiques de niveau recherche, publiés ou non, émanant des établissements d'enseignement et de recherche français ou étrangers, des laboratoires publics ou privés.

Copyright

Petrochronology and hygrochronology of tectono-metamorphic events

Valérie Bosse (1), Igor M. Villa (2)

(1) Laboratoire Magmas et Volcans, Université Clermont Auvergne, CNRS, IRD, OPGC, F-63000 Clermont-Ferrand, France; V.Bosse@opgg.univ-bpclermont.fr

(2) Institut für Geologie, Universität Bern, Baltzerstrasse 3, 3012 Bern, Switzerland; Centro Universitario Datazioni e Archeometria, Università di Milano Bicocca, pza della Scienza 4, 20126 Milano, Italy

Abstract

U-Th-Pb petrochronology is based on the incontrovertible fact that the diffusion of radiogenic Pb is negligibly small relative to retrograde reaction rates. Multi-element maps demonstrate that patchy textures tightly correspond to (U+Th)-Pb age variations, requiring that fluid-induced dissolution/ reprecipitation is the principal cause of Pb mobility. Attempts to model intracrystalline core-rim Pb zonations as diffusive transport are not legitimate unless genuine bell-shaped diffusion profiles in minerals can be documented, which happens only exceptionally. Monazite and zircon intra-grain age maps confirm that coupled dissolution-reprecipitation and retrogression reactions assisted by fluids control (Th+U)-Pb ages, not temperature. The chemical zonations observed in many (Th+U)-bearing mineral chronometers (e.g. monazite, allanite, xenotime, zircon) provide petrological constraints. Linking petrology with textures and the isotope record allows reconstructing entire segments of the *P-T-A-X-D-t* history of a rock and its geodynamic environment.

The dearth of mathematically sound diffusion profiles equally applies to the isotope record of micas and feldspars. The tight link between petrology, microtextures, chemical composition and geochronology also pertains to Rb-Sr and K-Ar. Overdetermined multi-mineral Rb-Sr isochrons with excess scatter, and spatially resolved/stepwise release ^{39}Ar - ^{40}Ar results, demonstrate ubiquitous correspondence between relict phases and isotopic inheritance. Many rock-forming minerals are highly retentive of Sr and Ar, unless they are obliterated by retrograde reactions. The rates of dissolution in fluid-controlled reactions are several orders of magnitude faster at upper and mid-crustal levels than diffusive reequilibration rates. Thus, as a rule Rb-Sr and K-Ar chronometers date their own formation.

Accurately establishing *P-T* paths of monometamorphic rocks requires assessing petrologic equilibrium using multivariate thermodynamic software. Dating complex parageneses of polymetamorphic, unequilibrated rocks requires labor-intensive disentangling by: (i) qualitative identification of relicts, retrogression reactions, and chemically open systems by imaging techniques (e.g. cathodoluminescence, element maps, etc.); (ii) microchemical analyses at the μm -scale quantifying heterochemical disequilibrium phases and assigning them to a *P-T-A-X* segment; (iii) spatially resolved/stepwise release, relating the chemical signature of the analyzed mineral to its age. K-Ar and Rb-Sr usually provide a different perspective on the *P-T* evolution of a rock than does (Th+U)-Pb, as K+Rb-rich minerals (phyllosilicates and especially feldspars) mostly form later and react/dissolve faster in the retrograde path than U-rich accessory phases (e.g. Mukai et al., 2014). The present

paper reviews these general principles by means of well-understood examples, both successful and unsuccessful in matching the independently known external constraints.

Introduction

Geodynamic models of the lithosphere seek to reconstruct the tectonic evolution and its duration. To this end, it is very useful to be able to link the information provided by microstructures to the petrogenesis of that same rock, and to connect both to the time information, to constrain the rates of crustal processes (Vance et al., 2003). The discipline connecting petrology and geochronology was later termed petrochronology (Kylander-Clark et al., 2013). Most metamorphic rocks record not just an instantaneous formation but a plurality of mineral-forming events, such that polymetamorphic and polycyclic rocks predominate in Pre-Cenozoic terrains. When studying Precambrian tectonics, field relations are often obscured by subsequent deformation, and petrological relations are often obscured by multiple metamorphic overprints. This makes tectonic models of Precambrian terrains especially vulnerable to the complexities of mineral geochronometers. The observation of relict minerals with abrupt compositional zonations, and in general of petrologic disequilibrium, poses a fundamental interpretive difficulty: assigning an age to each mineral generation, and linking each generation to the tectonic event that created the metamorphic conditions that led to its growth. Getting analytical data has become apparently easy. It is therefore important to improve the way that a mass spectrometric number is converted into a geological history and geodynamic context. This requires clarifying the approach used to interpret the geochronological data in order to increase the accuracy and reliability of tectonic models based on them.

A mineral is a useful petrochronometer if it fulfills two conditions: (1) its composition must be variable, in such a way that it records variable *P-T-A-X-D* (pressure-temperature-water activity-composition-deformation) conditions and allows tracing of chemically open-system behaviour; (2) its petrologic signature and its chronometry must be set simultaneously in the same geological event and remain unmodified ever since. When both conditions are fulfilled, it becomes possible to link the petrological and structural evolution of the chronometer to that of the rock, then on a larger scale to that of the geological unit, and finally to that of the orogenic belt.

The present review will discuss the kind of tectonic information that can be gained from geochronological data. To do so, it will address the fundamental assumptions underlying petrochronology by discussing examples of (Th+U)-Pb dating in monazite and K-Ar dating in micas in various tectono-metamorphic contexts. The studied examples show that (i) fluid assisted dissolution-precipitation processes rather than temperature-dependent solid diffusion predominantly govern the closure of the (Th+U)-Pb system; (ii) monazite is particularly sensitive to the interaction with fluids of specific composition (F, CO₂, K ...), even at low temperature; (iii) in the absence of fluids, monazite is able to record HT events and to retain this information during (poly-)metamorphism and even partial melting; (iv) patchy chemical and isotopic zonations, well known in monazite, reflect the fluid-assisted interaction with the surrounding mineral assemblages.

K-Ar chronometer minerals show similar patterns of isotopic inheritance closely tied to relict patches and heterochemical retrogression phases (Villa and Williams 2013). Isotopic closure in both (U + Th)-Pb and K-Ar systems follows the same principle: thermal diffusion is very slow, dissolution and reprecipitation are several orders of magnitude faster under typical crustal conditions. This means that both (Th+U)-Pb and K-Ar mineral chronometers are hygrochronometers. The petrochronological interpretation of the ages of the different domains cannot be decoupled from the geochemical and petrological context.

One crucial criterium for petrochronology are the relative rates of mineral-forming reactions and of diffusive reequilibration. A mineral that preserves both its major element composition and its radiogenic isotope signature has a petrogenetic stability field that allows its growth at temperatures lower than its "closure temperature" for diffusive loss of radiogenic isotopes as defined by Dodson (1973). Mineral petrochronometers all have this property (they were called "Class II chronometers" by Villa, 2016). In contrast, "Class I chronometers" (also called thermochronometers) are minerals that are open to diffusive loss of one or more daughter isotopes whenever they are formed, and only become closed to diffusive loss at a lower *T* than that at which they were formed.

The focus on petrology also implies, following Villa (1998, 2016), that the ages measured in petrochronometers from metamorphic rocks do not exclusively conform, in a mathematically invertible way, to the "closure temperature" concept (Dodson 1973). Examples of geodynamic models that only focus on the km-to-Mm scale and fail to take into account the atomic scale processes will also be discussed below. The only way forward is to bridge the gap between (sub-)µm-scale processes well understood by petrologists and mineralogists and km-scale processes addressed by tectonic models.

(Th+U)-Pb petrochronometry

Most Th±U-bearing minerals have high field strength elements (HFSE) as major cations, and inherently fulfill the requirement of efficient resistance to retrogradation and consequent degradation of the *P-T-A-X* information. One such mineral is monazite (Th, U, Ca, Y, Si, LREEPO₄), an accessory mineral in magmatic (mainly peraluminous and carbonatitic) and metamorphic rocks (mainly Ca-poor and Al-rich metapelites) where it represents one of the major reservoirs of lanthanides and actinides in the continental crust (Bea et al. 1996). Because of its wide range of possible cation substitution, monazite is a good tracer of the petrological events. Changes in the concentrations of Y, REE, Th, U reflect the partition of these elements between monazite and other minerals of the paragenesis that was in equilibrium at the time of monazite growth. Thermodynamic modelling allows to place monazite in a *P-T-A-X* grid (Mottram et al. 2014; Didier et al. 2015). However, integrating monazite in phase relations models and thermodynamic calculations is complex, because thermodynamic models remain highly dependent on the precise measurement of the trace elements in all the associated silicates.

Its high Th content (ThO₂ up to 15 wt% and more), and to a lesser extent U (UO₂ content < 2 wt%), allows the simultaneous use of three isotopic ratios (in order of abundance: ²⁰⁸Pb / ²³²Th, ²⁰⁶Pb / ²³⁸U, and ²⁰⁷Pb

Example 1. Monazite thermochronometry: the relevance of diffusion

Some workers (Steck & Hunziker 1994; Kohn 2013) have instead used monazite as a thermochronometer. The principal criterion to discriminate the legitimacy of this approach is the self-consistency of results, i.e. the modelling of a tectonic history that can be supported by geological arguments, independently of any circular argumentation based on isotopic data.

Steck and Hunziker (1994) compiled several dozen monazite and mica age data in a transect across the Central Alps. This is a very well mapped area, in which all the "canonical" calibrations of the "closure temperature" approach (Jäger 1967) were based. Steck and Hunziker (1994, their fig. 12) started from the assumption that all mica ages are "cooling ages". From this assumption, a chain of correctly applied logical implications implied two testable predictions: that the age of orogen-wide metamorphism was 38 Ma (the so-called "Leptontine metamorphism"), and that the "closure temperature" of monazite for Pb loss was 450 °C. The key argument for the latter estimate was the ubiquitous finding that $t_B < t_M < t_W$, t_B being the biotite K-Ar age, t_M the monazite U-Pb age and t_W the muscovite-whole rock Rb-Sr age (Fig. 3a). As monazite ages were younger than 38 Ma, their argument was apparently rounded off. However, the subsequent direct determination of Pb diffusivity in monazite (Cherniak et al., 2004; Gardés et al., 2006) established that monazite retains all of its radiogenic Pb* below 800 °C. This meant that all monazite ages in the Central Alps date the (diachronous) peak metamorphism, whose peak T did not exceed 650 °C, to the interval 15-25 Ma (Fig. 3b). The chain of arguments ought to be reversed: since t_W dates the metamorphic peak, any age higher than t_W contains a component of isotopic inheritance and must not be viewed as a "cooling age", negating the validity of the starting assumption. Inheritance affects most muscovite ages and a few biotite ages in an irregular geographic distribution, sometimes varying in the same locality (Arnold and Jäger 1965). The next implication is thus that retention of radiogenic ^{87}Sr and ^{40}Ar (hereafter $^{87}\text{Sr}^*$ and $^{40}\text{Ar}^*$) in relict micas can occur at 600 °C. This has a further corollary: as the thermal retentivity of micas is high, it is necessary to explain the rejuvenation of some (but not all) micas in the same, low thermal conditions by the predominance of a local, sample-dependent process: fluid-assisted recrystallization instead of temperature-controlled diffusion. Indeed, subsequent studies (e.g. Tartèse et al., 2011) document a tight parallelism between monazite and white mica ages, which can only be explained by interaction with aqueous fluids (see below).

The large-scale tectonic implications are a complete negation of the conclusions by Steck and Hunziker (1994). The metamorphic peak was not synchronous but diachronous in the different units. The relative movement of the units that are now juxtaposed in outcrop in the Central Alps persisted until later than 15 Ma. The average exhumation rate from peak pressure to outcrop is doubled. The cause for such a massive misinterpretation of Alpine tectonics was the assumption that monazite and micas were ideal thermochronometers. The assumed "closure temperature" of micas was (unrealistically) low, as in their samples it reflects not diffusion in a chemically closed environment but instead resetting by fluids at very low temperature. One extreme example of dating "white mica" in a petrologically careless/careful way is given by the muscovite-sericite reaction described by Maineri et al. (2003). These workers observed that white mica in

a related rock suite could come in two varieties: magmatic muscovite, aged 8.5 Ma; and sericite, reset at 7 Ma at a well-constrained temperature of 230 °C. If they had extrapolated the latter T-t point as a "thermochronological anchor point" of general validity for all white micas, regardless of their petrological origin, they would have estimated a "closure temperature" for white mica similar to, but slightly lower than, that proposed by Jäger (1967). Instead, by paying attention to the mineralogical reactions involving an aqueous fluid they were able to infer the correct sequence of events for Elba Island. In summary, the incorrect assumption that all mineral ages can be inverted to constrain a point in T-t space is bound to give incorrect tectonic reconstructions and unsubstantiated models of orogenic processes.

The discussion of the preceding example raises the question which, if any, mineral is a reliable thermochronometer, i.e. one in which the age is always controlled exclusively by diffusion, in such a way that age is always an invertible function of temperature. Diffusion is a very slow process, whose importance in natural rocks has been vastly overrated in the past (cf. the discussion by Villa and Hanchar, 2017, and the many references therein). The requirement stated in the Introduction, that the *P-T-A-X* signature and the isotopic age of a mineral should pertain to the same geological event, amounts to requiring that the diffusivity of the major elements (those on which the thermobarometry is based) must not be smaller than that of the radiogenic isotope that defines the age.

The mathematical equations for Fick's Law diffusion have a very simple outcome: diffusion always and only produces a bell-shaped (so-called error function, or erf) spatial concentration profile of the diffusant. If a genuine erf profile is observed, then probably Fickian diffusion was the predominant physical phenomenon in that sample (within the uncertainty of the fit of the data to the erf profile). If the spatial distribution of the diffusant resolvably deviates from an erf profile, then Fickian diffusion was not the predominant physical phenomenon, and numerical inversion models that assume Fickian diffusion are inaccurate and illegitimate.

The prime tool for the assessment of core-rim gradients in natural samples is by in-situ dating. In principle, in-situ techniques allow dating a mineral in its petrological-microstructural environment. In practice, an essential limit is the spatial resolution of in-situ analyses. There are two strict physical limits to the accuracy of an in-situ analysis. The upper limit of a useful primary beam diameter is given by the necessity to resolve the intergrowths of diachronous mineral generations in a complete way (Villa & Hanchar 2017, their figure 9). The literature abounds with reports that infer an incorrect age due to the uncorrected mixing of more than one mineral generation. The lower limit of a useful primary beam diameter is given by the necessity to average away the nm-scale recoil of radiogenic daughter nuclides by natural disintegration of the parent nuclide. Such atom-scale phenomena were documented in zircon by Kusiak et al. (2013), Valley et al. (2014) and Whitehouse et al. (2017) and in monazite by Seydoux-Guillaume et al. (2003) and Fougereuse et al. (2018), and result in a local disproportionation of parent and daughter nuclides. An unquestioning, context-less application of a single spot age obtained with a $< 1 \mu\text{m}$ primary beam would cause an incorrect age assignment of an entire orogenic cycle.

Studying older rocks by in-situ analyses has advantages and drawbacks. The advantage is that the number of radiogenic atoms that are required for precise dating is contained in a smaller volume. This allows

analyses with a higher spatial resolution and thus makes the dating of microstructurally distinct spots less difficult. The drawback is that the time-resolution provided by older rocks is less detailed than that of recent ones. A 1 % age uncertainty on a mid-Archean age, 30 Ma, is the duration of the entire Himalayan orogeny. Using in-situ analyses to tell apart events that lie 1 Ma apart is a serious challenge: for old rocks the analytical precision may be insufficient, for young rocks the spatial resolution may be insufficient to target only one generation of the petrochronometer mineral. Moreover, minor isotopes and/or trace elements are frequently below detection limit if the ablated volume is excessively small. This makes chemical fingerprinting of polyphase mixtures and heterochemical intergrowths difficult or impossible.

The disambiguation of mathematically correct erf profiles from generic core-rim zonation, such as e.g. accretion of a discrete heterochemical phase onto a relict core, requires a spatial resolution one or two orders of magnitude better than the length scale of the zonation. Moreover, if one element exhibits a genuine diffusion gradient in a mineral, then all elements whose boundary conditions allow it must exhibit one as well. Since the diffusion length is proportional to \sqrt{Dt} , where D is the diffusion constant and t is the duration of the heating event, all diffusing elements from the same mineral grain must necessarily exhibit diffusion length scales that depend on the (well predictable) relative diffusion coefficients.

Neglecting the systematic dependence of diffusivity on charge and radius is not just an academic detail, as it can lead to unrealistic tectonic modelling. As an example, Ewing (2017) used Zr-in-rutile thermometry to determine metamorphic peak temperatures of ca. 850-950 °C in lower crustal granulites from Corsica (France). They then dated the rutile by U-Pb and assumed that their age, 160 Ma, was a "cooling age" corresponding to exhumation of the rutile through the 550-650 °C isotherm. This was interpreted as evidence of the exhumation of the lower crust during the formation of the first oceanic crust in the Late Jurassic. However, a few independent constraints conflict with this tectonic model. Firstly, the Jurassic evolution of the geotherms in the entire Corsica-Sardinia block is constrained by fission tracks and U*-He ages (Malusà et al. 2016), whereby the oceanic crust was already being thrust over the continent ca. 10 Ma earlier. Secondly, the lower crust had already been exhumed during the Permian; during the Jurassic rifting the thermal perturbation was weak (Malusà et al 2016). The misunderstanding of diffusion systematics by Ewing (2017) was subtle. The Zr-in-rutile thermometer was assumed to reliably record the peak temperature, which means that the Zr concentration was not modified by diffusive re-equilibration. ~~On the contrary,~~ The ionic radii of Zr^{4+} (86 pm) and Pb^{4+} (91.5 pm) predict that Pb^* diffuses much less fast than Zr, i.e., if Zr-in-rutile records a formation temperature then the U-Pb age of rutile must a fortiori record a formation age.

A multichronometric assessment of the internal consistency of models that interpret mica ages following thermochronology was recently reported by Airaghi et al. (2018). Biotite and allanite grew synchronously during burial, and both chronometers give mutually concordant ages between 220 and 180 Ma. The chronometric information recorded by both minerals survived metamorphic peak temperatures of c. 580 °C. Retrograde muscovite formed around 130 Ma at c. 370-470 °C (whereby the size mismatch, discussed above, between "small" mineral grains and "large" laser beam prevents reproducible dating of separate muscovite generations: Airaghi et al., 2018, p. 947). Diffusion modelling is unable to reproduce any of these observations (Airaghi et al., 2018, p. 954), as predicted by Villa (2016, p. 8). What the allanite and mica

multichronometry really means is that "petrological and microstructural processes prevail over thermally driven diffusion even at high temperatures" (Airaghi et al., 2018, p. 954), which puts new, robust constraints on the Triassic-Jurassic tectonics of the Longmenshan orogen.

In a very recent paper, Kirkland et al. (2018) analyzed compositional and Pb isotopic profiles in apatite. They concluded that "To apply Pb diffusion profiles to determine cooling histories, one must not assume but demonstrate that thermally activated volume diffusion is justifiable because our results show that apatite generally may not record simple thermally activated Pb diffusion profiles but rather profiles modified in part or whole by recrystallization or new growth" (Kirkland et al., 2018, p. 155).

As evidenced by the three just cited 2017-2018 papers, observations of erf profiles in natural geological systems are very rare (confirming the references cited by Villa 2016). More frequent are the observations of "slow" diffusion being overtaken by superimposed faster processes, such as dissolution/reprecipitation in aqueous fluids (e.g. Labotka et al. 2004, their Fig. 4). The relative magnitude of the rate constants of diffusion and of dissolution also affects very heavily the literature estimates of the geochronology of micas and feldspars. The discussion by Villa (2016) needs not be repeated here; the observation most relevant for the present discussion is that, in the absence of dissolution/reprecipitation due to aqueous fluids, the "dry" diffusivity of the radiogenic daughters in micas ($^{40}\text{Ar}^*$ and $^{87}\text{Sr}^*$) is sufficiently low to make these minerals Class II geochronometers.

Beyond (Th+U)-Pb: Rb-Sr and K-Ar

The reasons why micas are petrochronometers in the Rb-Sr and K-Ar systems must be sought at the atomic scale. Ar is a very large atom (its van der Waals radius $r_{\text{Ar}} = 188$ pm, much larger than oxygen and the structure-forming cations) with a high polarizability. It does not form true bonds but can be adsorbed onto a surface by van der Waals forces, with an activation energy around 10 kJ/mol. Sr^{2+} is even larger and less adapted to the silicate framework (its covalent radius $r_{\text{Sr}^{2+}} = 195$ pm). Pb^{4+} is also very large, and due to its high charge (Kramers et al. 2009) it is one of the slowest diffusants.

Definitely a single Ar atom is not a "noble gas" in the thermodynamic sense. The properties of a gas are manifested when there are a few millions other free gas atoms, all of whom obey the equations of statistical mechanics. On the other hand, when an individual Ar atom is trapped interstitially within a solid as a single atom it is so impeded in its movement that Boltzmann's Law [$v \sim \sqrt{kT}$] does not apply. The threshold for gaseous behaviour is reached when the mean free path of the atoms at the T of interest is smaller than the size of the cavity it is confined in. This corresponds to a few hundred nm inclusions (depending on the entrapment P and T). When the inclusion's internal overpressure, given by $P=nRT/V$, exceeds the strength of the solid host, can the trapped atoms be released as a gas by decrepitation.

Just as evidently, an Ar atom trapped in a solid is not a Fickian diffusant. After decades of confusion, it has become clear that the measured activation energies for Ar transport provide unambiguous constraints on where, how and why an Ar atom can migrate. Ar makes no bonds with structure-forming cations, nor with

oxygen, and thus should have a partition coefficient near zero. Other than in (passively trapped) fluid inclusions, ^{40}Ar never comes into a crystal except as the radiogenic daughter, $^{40}\text{Ar}^*$, of a ^{40}K atom that captured one of its 1s electrons. When the excited $^{40}\text{Ar}^*$ isomer decays to the ground state, it emits a gamma photon with an energy of 1.46 MeV. By momentum conservation, the $^{40}\text{Ar}^*$ nucleus recoils by tens of nm, during which movement it probably also undergoes recoil stripping of a few of its electrons. Thus, the $^{40}\text{Ar}^*$ ion is no longer located in the same crystallographic location as its parent isotope ^{40}K . Its positively charged state is metastable and the electrical neutrality might be recovered quickly, but no experimental data exist so far.

A further argument against the free mobility of rare gases through the mineral structure is the very different diffusivity and activation energy of Ar and Xe. Hetherington and Villa (2007) measured the degassing rate of irradiated celsian, in which neutron-produced ^{39}Ar and ^{131}Xe were measured simultaneously. If both had been free to move, both should exhibit similar activation energies, of the order of the van der Waals binding energy. Instead, the observed activation energy of Ar in celsian was 180 kJ/mol, similar to that of alkali diffusion, whereas the observed activation energy of Xe was 330 kJ/mol, similar to that of Ba diffusion.

The energy budget of Ar migration in natural solids is extremely difficult to measure. Mineral chronometers relevant for the K-Ar system are mostly hydrous (amphiboles, micas), feldspars being the anhydrous mineral most widely used as a chronometer. At this time, the reliable estimates of Ar diffusivity in natural mineral chronometers can be counted on the thumbs of one hand. Experiments on hydrous minerals return the dissolution/precipitation rate (Villa, 2010, 2016) instead of the Fick's Law diffusivity. Experiments on feldspars (Wartho et al., 1999) can return a true diffusivity only provided the sample is ideally monomineralic. Polyminerale samples return average properties of the sum of all coexisting phases (Chafe et al., 2014). Despite the general unreliability of literature estimates for Ar diffusivity, a few guidelines can orient users through the apparent disorder of the database: (i) diffusion occurs always, but is always the slowest transport mechanism (Villa, 2016; Villa and Hanchar, 2017 and references therein); (ii) the similarity of activation energies for dissimilar diffusants is proof that the limiting factor in diffusion are the properties of the matrix structure, in particular the creation of Schottky vacancies that allow the movement of cations across the structure; (iii) the vast variations in frequency factors, i.e. of the likelihood that a given ion will exploit the newly created Schottky vacancy, are a function of charge and radius of the diffusant: larger ions have lower frequency factors (Chakraborty and Ganguly, 1992), as do ions with a higher charge (Cherniak 2006, 2010).

The Rb-Sr ages reported in the references quoted by Steck and Hunziker (1994) are affected by an additional problem besides the relative role of diffusion and recrystallization. The cited mica Rb-Sr ages were all two-point mica-whole rock isochrons. Two-point isochrons may assign a not entirely incorrect general geological era, but their accuracy relies on the isotopic equilibrium between the two analyzed data points. In the case of a metamorphic system, the whole rock always contains relict phases and retrogression products, which guarantees an incomplete isotopic equilibrium and a questionable accuracy of isochrons. When metamorphic rocks are dated by Rb-Sr it is necessary to obtain overdetermined internal isochrons by analyzing a large number of coexisting minerals. The cogeneticity manifests itself by a low dispersion of the data points,

In metamorphic reactions, fluid-assisted processes are not the exception, but rather the rule (Putnis 2002, 2009; Putnis and John 2010). Fluids play a catalytic role by decreasing the activation energy of a reaction and by promoting the dissolution/precipitation processes and material transport. Even at HT conditions in eclogite and granulite conditions, Putnis and Austrheim (2013) showed that the availability of fluids is an essential condition for the metamorphic reactions to proceed, whereas solid-state reactions only involving volume diffusion are not the dominant mechanism (see also Mukai et al., 2014; Centrella et al., 2016). Finally, these authors question the difference between metasomatism and metamorphism and conclude that there is no fundamental difference between the two processes at the molecular scale: metamorphism involves fluids, albeit at local scale and lower volume. Thus, ~~to~~ dating the fluid circulation events associated with the formation of a metamorphic paragenesis requires the use of hygrochronometers.

Monazite is well known for its high reactivity in presence of fluids even at low temperatures (Poitrasson et al. 1996; Teufel and Heinrich 1997; Townsend et al. 2001; Seydoux-Guillaume et al. 2002; Bosse et al. 2009; Harlov and Hetherington 2010; Hetherington et al. 2010; Harlov and Hetherington 2011; Williams et al. 2011; Budzyn et al. 2011; Didier et al. 2013): the dissolution/recrystallization processes ubiquitously observed in metamorphic rocks induce the formation of intra-grain monazite domains of distinct age and chemistry, whatever the thermal conditions. Monazite should therefore be called a hygrochronometer. In fluid-assisted dissolution-precipitation processes, precipitation is usually spatially associated with dissolution along the dissolved interface (Putnis 2002). The newly formed monazite usually crystallizes as a more or less discontinuous overgrowth surrounding the primary crystal (see for example Fig. 8 and 9). This is the result of the often restricted mobility of the monazite major elements and induce porosity development, total or partial preservation of the initial grain shape (pseudomorph) and mixing between successive monazite generations at small scale (<500 nm) (Fig. 6; Grand'Homme et al. 2016). This highlights the heterogeneous character of the monazite at the nanoscale observed by atom probe and TEM imaging (Fougereuse et al. 2018; Grand'Homme et al. 2018), and at the same time confirms the negligibility of diffusive reequilibration. Monazite reactivity mainly depends on the *A-X* of the interacting fluid rather than *P-T* conditions (Seydoux-Guillaume et al., 2002 ; Teufel and Heinrich, 1997; Hetherington et al., 2010). Experimental studies show that fluids rich in F, CO₂, Ca, and alkali strongly influence the stability of monazite (Hetherington et al., 2010, Harlov and Hetherington, 2010; Harlov and Hetherington, 2011, Budzyń et al., 2011, Richard et al., 2015) and the mobility of Th, U and Pb. Didier et al. (2013) report Th/U fractionation during hydrothermal processes in presence of F-rich fluids with attending age disturbances. Both Th and unradiogenic Pb were independently enriched in variable proportions in the hydrothermal monazite (Fig. 7). This led, in the case studied, to meaningless ²⁰⁸Pb/²³²Th ages, some becoming older by the effect of excess Pb, and some younger by late-stage incorporation of Th. As the U content remained nearly constant, the ²⁰⁶Pb/²³⁸U ratio also scatters, due to external Pb incorporation. A similar behavior has been described with various fluid composition by Janots et al. (2012), Wawrzenitz et al. (2012) and Grand'Homme et al. (2018).

During metamorphic reactions, the fluid composition is mainly controlled by local equilibria and depends on the reactivity of the other major and trace minerals involved in the reactions. Because fluid composition also strongly controls the behavior of the monazite during dissolution/recrystallization processes,

it is not possible to predict a priori in which direction the Y, REE, Th, U or Pb content will change. Thus low or high-Y or Th content in monazite domains cannot be used a priori as tracers of specific metamorphic conditions (as proposed by Kohn, 2016) in order to attribute ages measured in the same domain to specific metamorphic stages. *P-T-A-X* conditions must instead be calibrated independently for each metamorphic reaction on a case-by-case basis, using the compositions of monazite and of other reactants. With such extensive work, the monazite can be used as a powerful tracer of the tectono-metamorphic events. The recrystallized domains synchronously record the age and the *A-X* conditions at the time of their formation. This allows precise dating of tectonic or metamorphic, successive or polycyclic events. The following examples illustrate the effectiveness of the monazite hydrochronometer for that purpose.

Example 3. Dating deformation

Because of the inherent scale limitations of in-situ techniques, direct dating of microstructures in metamorphic rocks remains a challenge (Williams and Jercinovic, 2002; Wawrzenitz et al. 2012; Dumond et al. 2013; Erickson et al. 2015). Dating of deformation first requires a geochronometer mineral showing microstructural evidence of (re)crystallization following the. Secondly, the chemical composition of the geochronometer must reflect the metamorphic conditions taking place during deformation, taking care to recognize and exclude relict grains or inherited subgrains having crystallized before the deformation event. Last but not least, there is the difficulty of resolving the ages of events that are close in time. The didactically illuminating examples provided by Williams et al. (2011) pertain to the discrete Proterozoic overprint of an Archean rock in the Athabasca granulite terrain (Canada) in a separate orogeny. The next challenge is now constraining the petro-hydrochronological sequence of the prograde and retrograde *P-T-A-X-D-t* segments of a single orogenic cycle in the Meso-Cenozoic as an actualistic tool to better understand Precambrian orogenies.

Didier et al. (2014) observed deformation textures in monazite grains and dated the deformation events by coupling monazite geochronology with a detailed petrological and structural study. This study focuses on garnet-kyanite (Grt-Ky) metapelites embedded within two major shear zones of the central part of the Rhodope Metamorphic Complex (Greece, Bulgaria) : the Nestos shear zone (NSZ) in Greece and the Chepelare shear zone (CSZ) in Bulgaria. Samples from both locations have experienced two stages of high temperature metamorphism during Alpine times. The first event involved mid-Mesozoic upper amphibolite - granulite facies « dry » melting. The second event involved mid-Cenozoic lower amphibolite fluid-assisted partial melting. All samples, despite some petrological differences, show microstructural evidence for strong ductile shearing in the presence of fluids. Monazite is abundant as inclusions in garnet and kyanite and in the highly foliated matrix. The matrix grains show strong evidence that at least part of their growth occurred during deformation: i) crystallization channeled along muscovite cleavages (Fig. 8a and e), small satellite grains surrounding larger monazite grains (Fig. 8b), iii) clusters of contiguous small grains possibly replacing an older grain (Fig. 8c) or strings of small monazite grains parallel to the matrix foliation (Fig. 8d). These monazites are commonly associated with rutile (Fig. 8e) and biotite grains which also crystallized along the cleavage planes of the host muscovite (Fig. 8c) or in asymmetric strain shadows around garnets. All these

textural characteristics of monazite suggest a syn-deformation fluid-assisted monazite growth. Matrix monazite also displays strong chemical and isotopic zoning : the large Y-poor cores yield mid-Mesozoic ages (ca. 115 and 165 Ma), similar to the monazite inclusions in garnet and kyanite, and the thin, commonly irregular Y-rich rims yield Cenozoic ages (ca. 36 Ma) (Fig. 9). The small Y-rich monazite grains parallel to the main foliation also display Cenozoic ages. These observations clearly show that new syn-deformation monazite generation formed at ca. 36 Ma as the result of fluid-assisted inter-grain mass transfer.

Mesozoic monazite is the main precursor of the new monazite generation. Hence, a process of dynamic dissolution–reprecipitation, as described by Wawrzenitz et al. (2012), probably accounts for the growth of the Cenozoic monazite: the chemical composition of the new grains record the metamorphic conditions of the new environment during deformation, and the shape of the monazite grains indicates the sense of shear, thus linking the measured ages directly to the map-scale tectonic transport. Sharp boundaries separating the chemical domains of distinct ages testify that old monazite grains survive the intense fluid-assisted deformation and are totally preserved. Diffusion processes were not effective. Clearly, the record of the deformation age is the result of dissolution-recrystallization processes rather than intracrystalline temperature-dependent diffusion of trace elements.

In the Rhodope samples, the recrystallization of monazite occurs at $P \approx 8\text{--}10$ kbar and $T \approx 650$ °C. But dissolution – recrystallization of the monazite is also known to be possible at lower grade conditions. In the Variscan Agly massif localized in the North-Pyrenean zone (Eastern Pyrénées, France), Variscan monazite in para- and ortho-gneisses sampled in mylonitic shear zones displays recrystallized domains of Cretaceous age (125–110 Ma) related to the Albian extension between the Iberian and European plates. In these samples, fluid-assisted deformation occurs at decreasing temperature conditions from $T > 550$ °C to $T \approx 200$ °C. Younger ages (c. 110 Ma) are associated with brittle deformation whereas older ages (c. 125 Ma) are associated with ductile microstructures suggesting a continuous record of the deformation during the cooling and the exhumation of the Agly massif in the Cretaceous times (Aumar, 2018). It is important to note that Cretaceous ages have been only recorded in syn-tectonic minerals such as monazite, titanite ((Th+U)-Pb system) and micas (K-Ar system) (Chelalou et al. 2016; Nicolas, 1998), but not in zircon. Outside the shear zones, Variscan monazites are preserved. These examples again document that fluid-assisted recrystallization during deformation is responsible for the isotopic closure of the (U+Th)-Pb and K-Ar systems in minerals that actively participate in metamorphic reactions.

Example 4. Polyclism and polymetamorphism

Crystalline complexes occasionally feature rocks having experienced polycyclic metamorphism during several successive orogenies and/or other geodynamic settings. Polyclism needs to be distinguished from continuous successive stages of a P - T path during a single orogenic cycle (Gautier et al. 2017). The possible identification of several stages of deformation or successive metamorphic parageneses may only reflect the complex evolution of a single orogen. Geochronological data may give the best evidence of polyclism,

532 provided that these are closely related to structural and petrological data. In contrast, an erroneous attribution
533 of some ages to structures and/or metamorphic assemblages can lead to a wrong tectonic interpretation. This is
534 especially the case for polycyclism, as specific metamorphic conditions (e.g. eclogitization or migmatization)
535 related to an old orogeny may be attributed to a younger one. However, dating the mineral assemblages
536 corresponding to distinct metamorphic events in the same rock is never easy, especially when *P-T* conditions
537 of these events are close. This is the case for the Grt-Ky metapelites described above (Didier et al., 2014), for
538 which a detailed petrological study did not allow rigorous identification of two Mesozoic and Cenozoic
539 parageneses. Only matrix monazite was able to record the two successive events, thanks to the presence of
540 fluids during the deformation in Cenozoic times.

541 Another example of polycyclism recorded by monazite is given by the study of coronitic paragneisses
542 in the Les Essarts high-pressure unit, which occurs in the Southern Armorican Massif (Vendée, Western
543 France). It delineates a NW–SE-trending zone about 70 km long and a few km wide, between two late-
544 Variscan dextral faults (e.g., Godard, 2001, 2009). It comprises eclogite and amphibolite derived from
545 eclogite, which form lenses several km long, stretched and boudinaged in ortho- and paragneisses. The host
546 coronitic paragneisses have undergone a complex evolution: high-*T* metamorphism ($T \approx 670\text{ }^{\circ}\text{C}$, $P \approx 0.32$
547 GPa) followed by retrogression during Proterozoic times and eclogite-facies overprint ($T \approx 700\text{ }^{\circ}\text{C}$, $P \approx 1.6$
548 GPa) and final retrogression during Variscan times (Godard, 2009). The second episode gave rise to many
549 pseudomorphic and coronitic reactions and caused high-pressure minerals to grow at the expense of the
550 previous high-temperature parageneses. Monazite is highly abundant in the coronitic paragneisses. Some
551 samples show disequilibrium textures with the surrounding matrix minerals. Apatite-bearing coronas around
552 monazite only developed at contacts with plagioclase following the reaction : $\text{Mnz1} + \text{Pl (LP - HT)} = \text{Mnz2} +$
553 $\text{Ap} + \text{Zo (HP - LT)}$ (Fig.10a). This gives us the opportunity to date the different metamorphic events in these
554 samples. Very small chemical differences are observed between the core of the M1 monazite grains (c. 30 to
555 $>100\text{ }\mu\text{m}$ in size) and the small M2 monazite grains in the corona ($<5\mu\text{m}$ in size). This argues in favour of
556 very limited element transport during the reaction and in situ dissolution/reprecipitation processes. Regarding
557 the geochronological data, three different groups of ages can be distinguished. Few data yield concordant Th-
558 U-Pb ages in the monazite cores at around 590 – 600 Ma, whereas the majority of the measured ages is at
559 around 485 Ma (Fig. 10b; Bosse et al. 2010). The third group corresponds to the M2 monazites in the corona.
560 Because of the small size of the M2 grains relative to the laser spot size ($5\text{ }\mu\text{m}$), which induces a variable
561 amount of mixing with the adjacent minerals and unradiogenic Pb contamination, most of the M2 analyses are
562 discordant. The few concordant ones are highly scattered. Thus constraining the age of the HP event in these
563 samples was not easy mainly for technical reasons (i.e. the laser spot size) and the results are not very precise,
564 between 400 and 350 Ma. The most striking feature here is that, despite the complexity of the petrological
565 context (i.e. the presence of multiple and varied pseudomorphs and coronas), the early monazite retains its
566 primary chemical and isotope characteristics. It only partially recrystallizes via in situ
567 dissolution/reprecipitation during HP metamorphic (possibly dehydration) reactions. In neighbouring samples
568 following the same petrological evolution, when monazite coronas are absent, the HP Variscan event is not

recorded by the monazite. This demonstrates that petrological processes governed the closure of isotopic systems in monazite and ages obtained in monazite date its ~~own~~ crystallization.

For this reason, monazite is a very good tracer of the petrological processes, unlike zircon, which cannot easily be used as a petrochronometer. As it is usually associated with allanite, apatite or xenotime, with which it shares its constituent elements, monazite exhibits textures that directly reflect the metamorphic reactions. Thus dating successive metamorphic stages following the prograde or retrograde sequence of rare earth minerals along a single polymetamorphic orogenic cycle is quite easy, providing in situ ages in microstructural context. Some nice examples exist in the literature (Janots et al. 2008; Janots et al. 2009; Regis et al. 2014). Skrzypek et al. (2016) provide textural and geochronological arguments to constrain monazite petrogenesis and the age of metamorphic events in medium-grade metasedimentary rocks from the Orlica-Śnieżnik Dome (Czech Republic/Poland). A first monazite generation formed via allanite breakdown during garnet growth at prograde to peak P - T conditions (5–7 kbar, 575–640 °C) at around 360–340 Ma. Retrograde processes are responsible for the dominant monazite age population of 330–310 Ma ascribed to a combination of (1) transient monazite growth after allanite and controlled by P availability, (2) variable recrystallization/ replacement of older monazite grains, and (3) minor monazite neoformation due to the resorption of garnet or apatite. These successive episodes of monazite growth evidence the metamorphic reactions involving major and trace minerals during one single orogenic cycle.

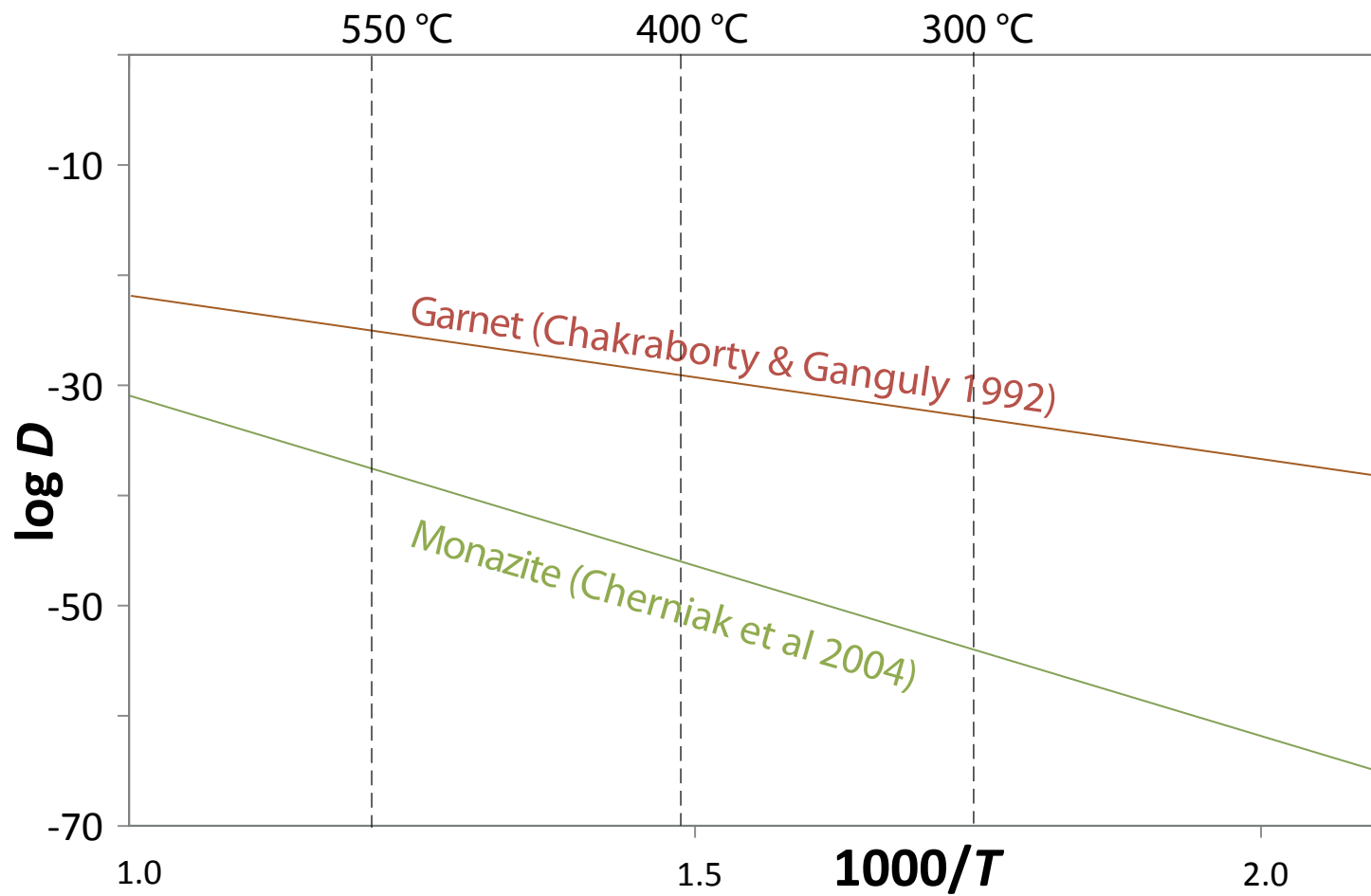
If the reactions involving petrochronometers and major phases are well identified and calibrated in terms of P - T - A - X conditions, and only in this case, they can be used to calculate duration or exhumation rates. As a recent example, Manzotti et al. (2018) propose to evaluate the exhumation rate of the Gran Paradiso and Monviso Units (Western Alps) by studying the relative timing of the growth and dissolution of the accessory phases. Combining thermodynamic modelling with HP inclusion, textural and chemical data from both major and accessory phases, these authors were able to date the metamorphic peak and retrograde evolution by fixing P - T conditions of the crystallization episodes of allanite, monazite and xenotime (Fig. 11). The whole set of petrochronological data allow to constrain an exhumation rate of the order of 2.2–5 mm/a for these HP units. This type of approach gives results that substantially differ from calculations only based on closure temperature estimations. As the P - T signature and chronometry are simultaneously constrained, the results allow much more accurate geodynamic models.

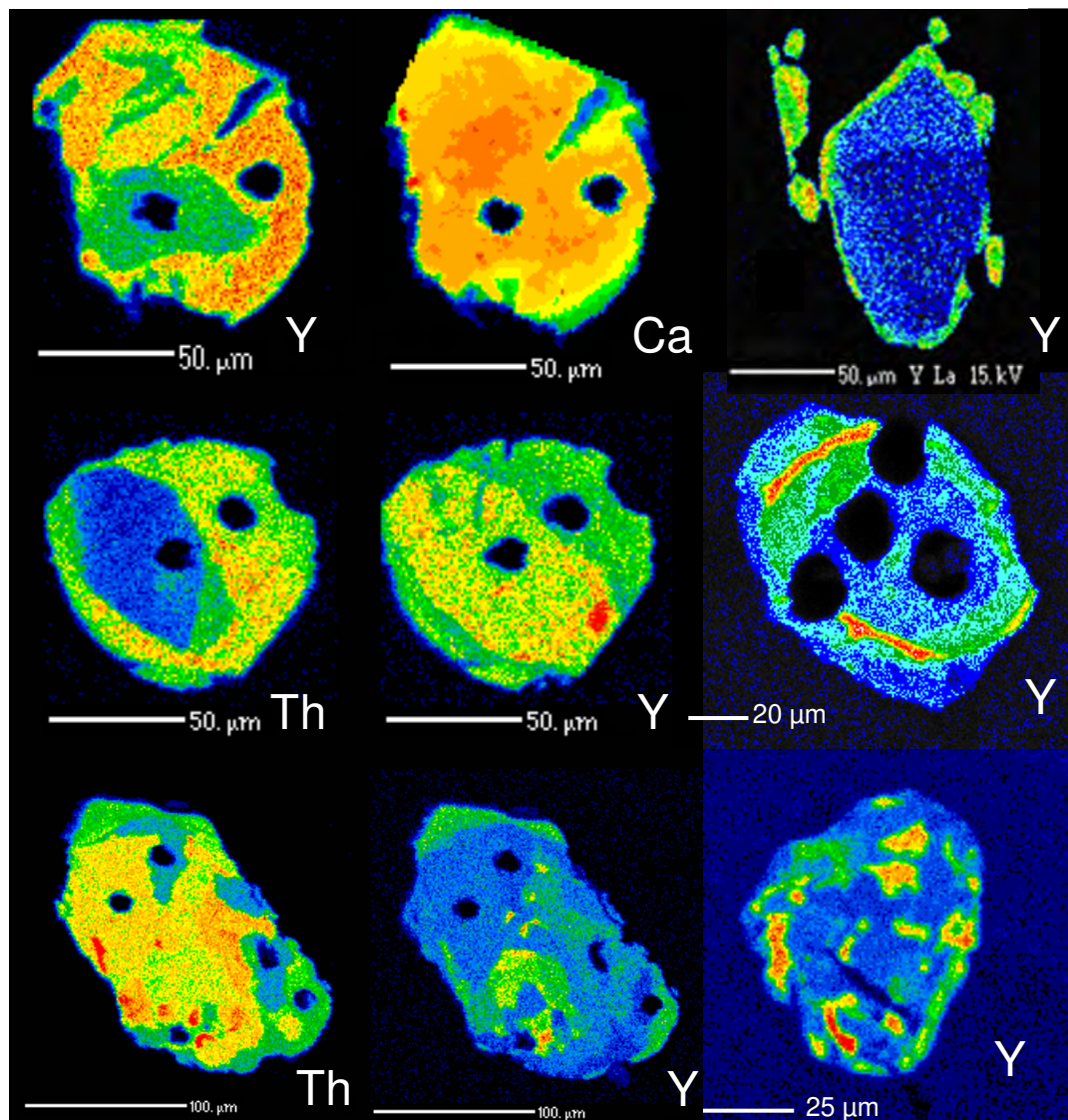
Concluding remarks

1. Tectonic models are only as good as the weakest link in the quantification of a P - T - A - X - D - t path.
2. Texture-oriented, high-resolution petrography discriminates equilibrium parageneses from fluid-infiltrated, retrogressed portions of mineral grains and from relict phases.
3. Polygenetic assemblages provide petrochronological constraints if both the petrological and the chronological record are pristine. The examples presented of monazite and mica petrochronometry illustrate

BSE image and corresponding LA-ICPMS $^{208}\text{Pb}/^{232}\text{Th}$ ages (spot size $5\mu\text{m}$, 2σ uncertainty) (Bosse et al. 2010)

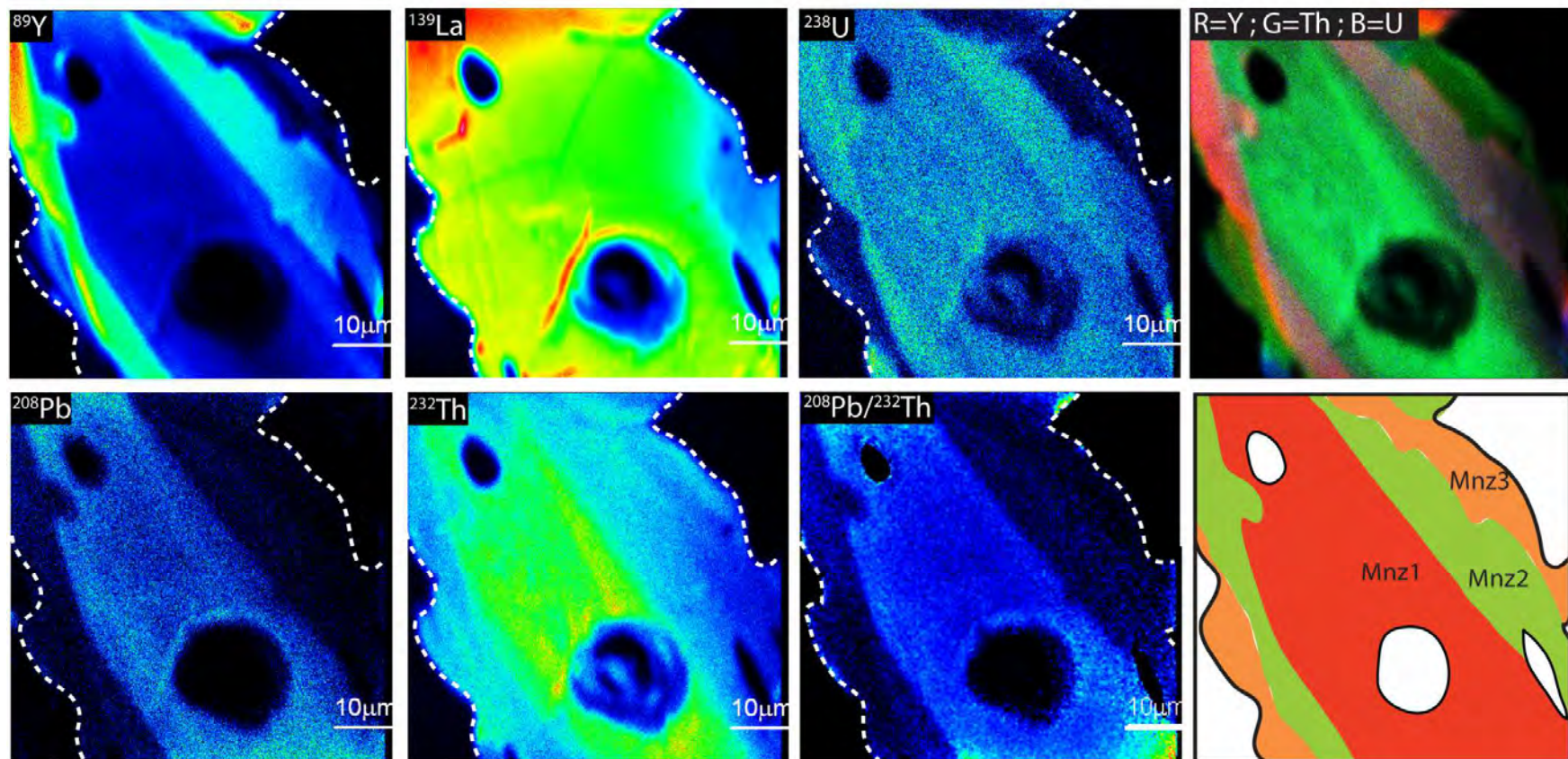
Fig. 10 - Summary of the petrochronological results (P–T paths and monazite $^{208}\text{Pb}/^{232}\text{Th}$ ages). Note the presence of HP inclusions, which confirm the crystallization of the monazite during HP metamorphism conditions. Money Units (a) and Gran Paradiso (b), modified after Manzotti et al. (2018).





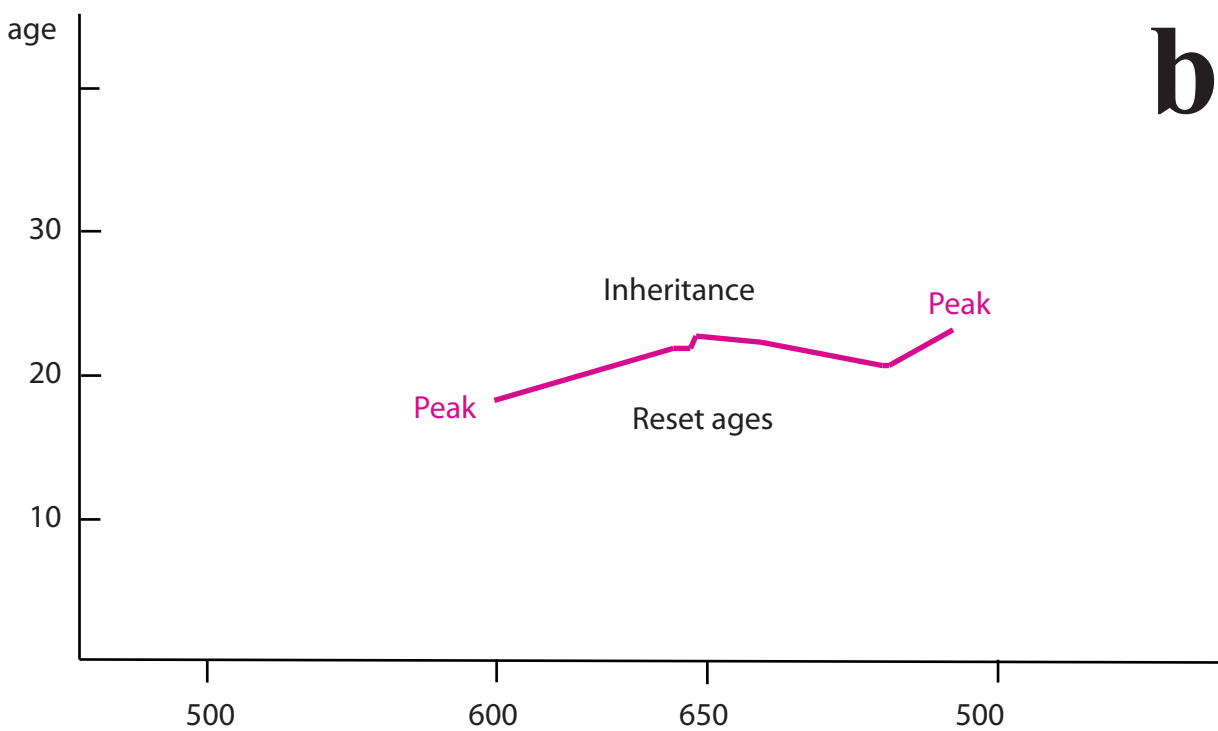
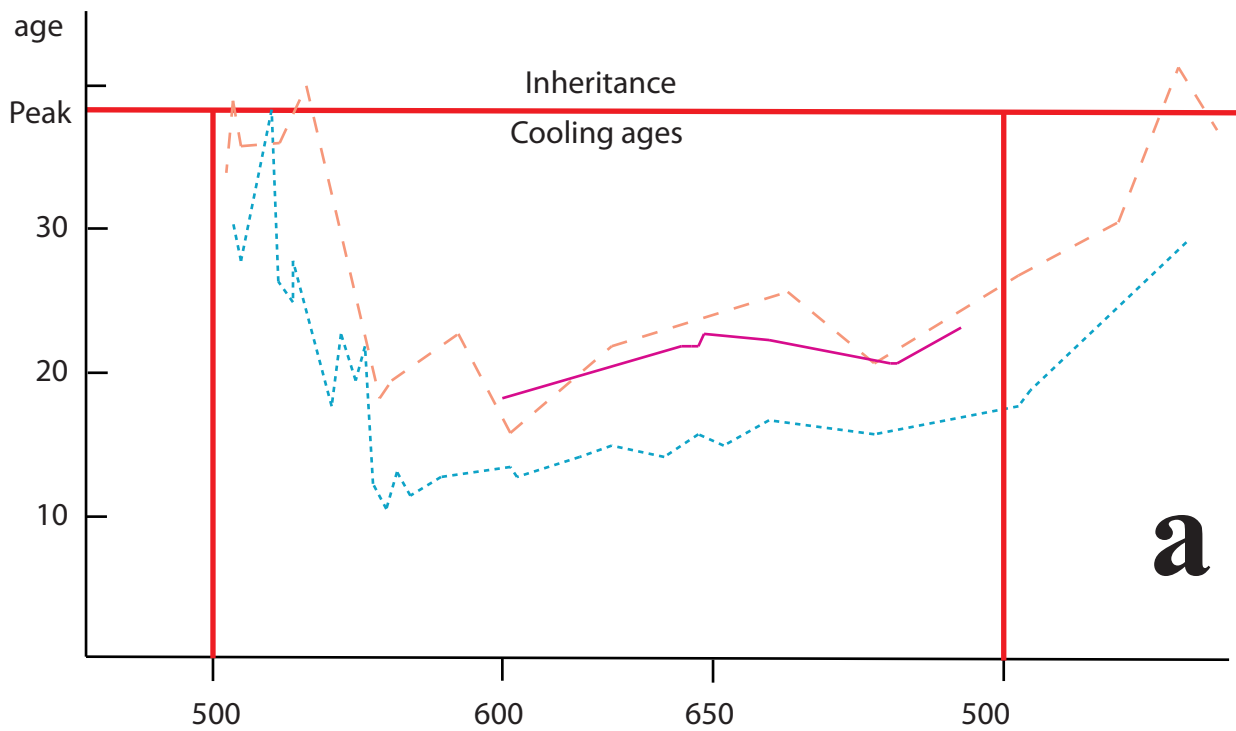
Different types of monazite zonation (EMP X ray maps). (Didier et al. 2014; Didier et al. 2015; Bosse et al. 2009)

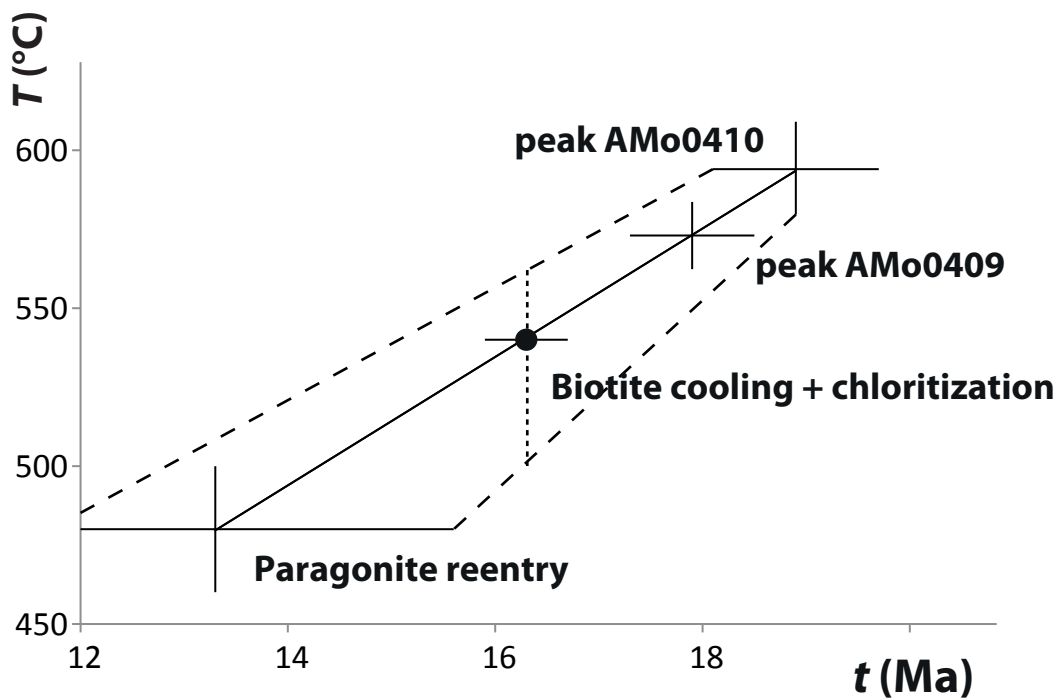
Fig. 2a



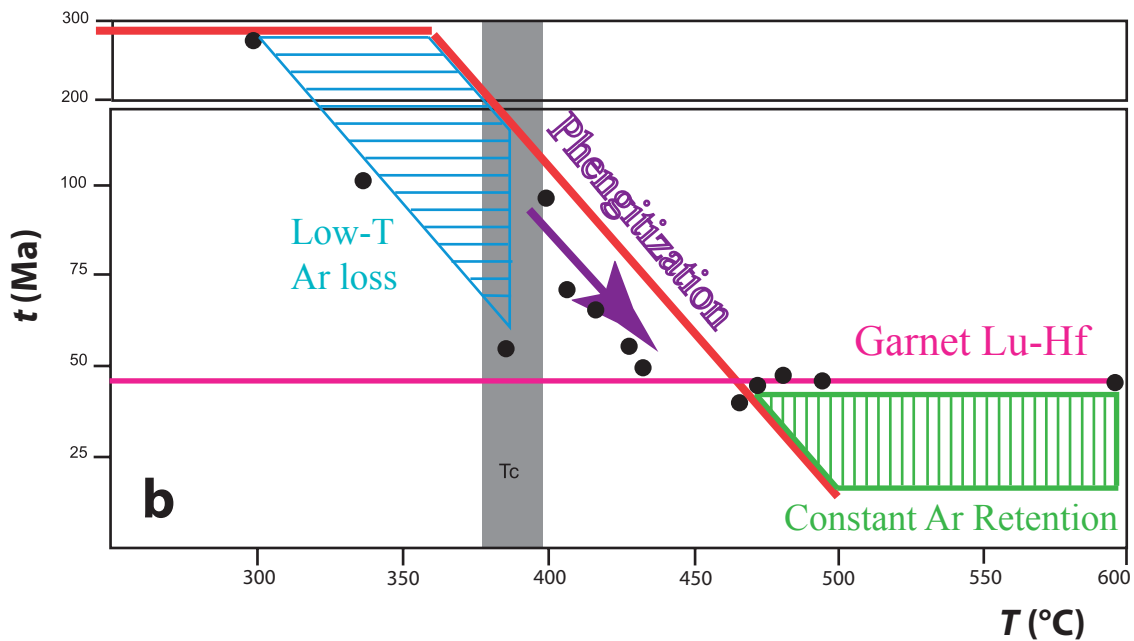
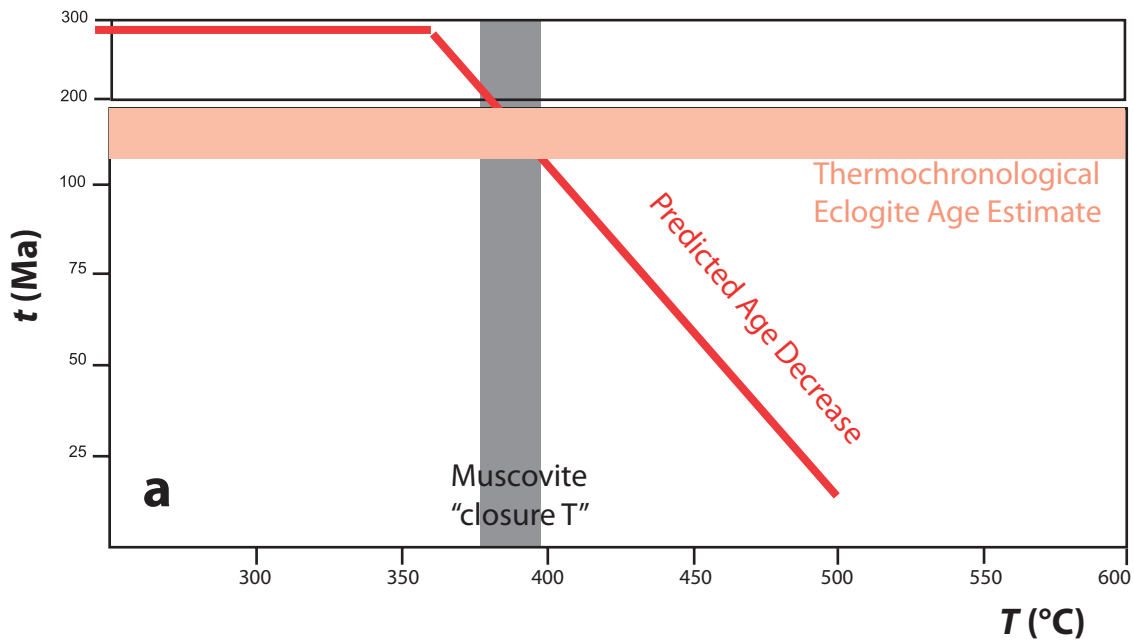
NanoSIMS distribution maps (^{89}Y , ^{139}La , ^{238}U , ^{208}Pb , ^{232}Th and $^{208}\text{Pb}/^{232}\text{Th}$), RGB maps (Y in *red*, Th in *green* and U in *blue*) and interpretive sketches of selected portions of Monazite. The sketches distinguish between the M1 (*red*), M2 (*green*) and M3 (*orange*) domains. Didier et al. (2015)

Fig. 2b

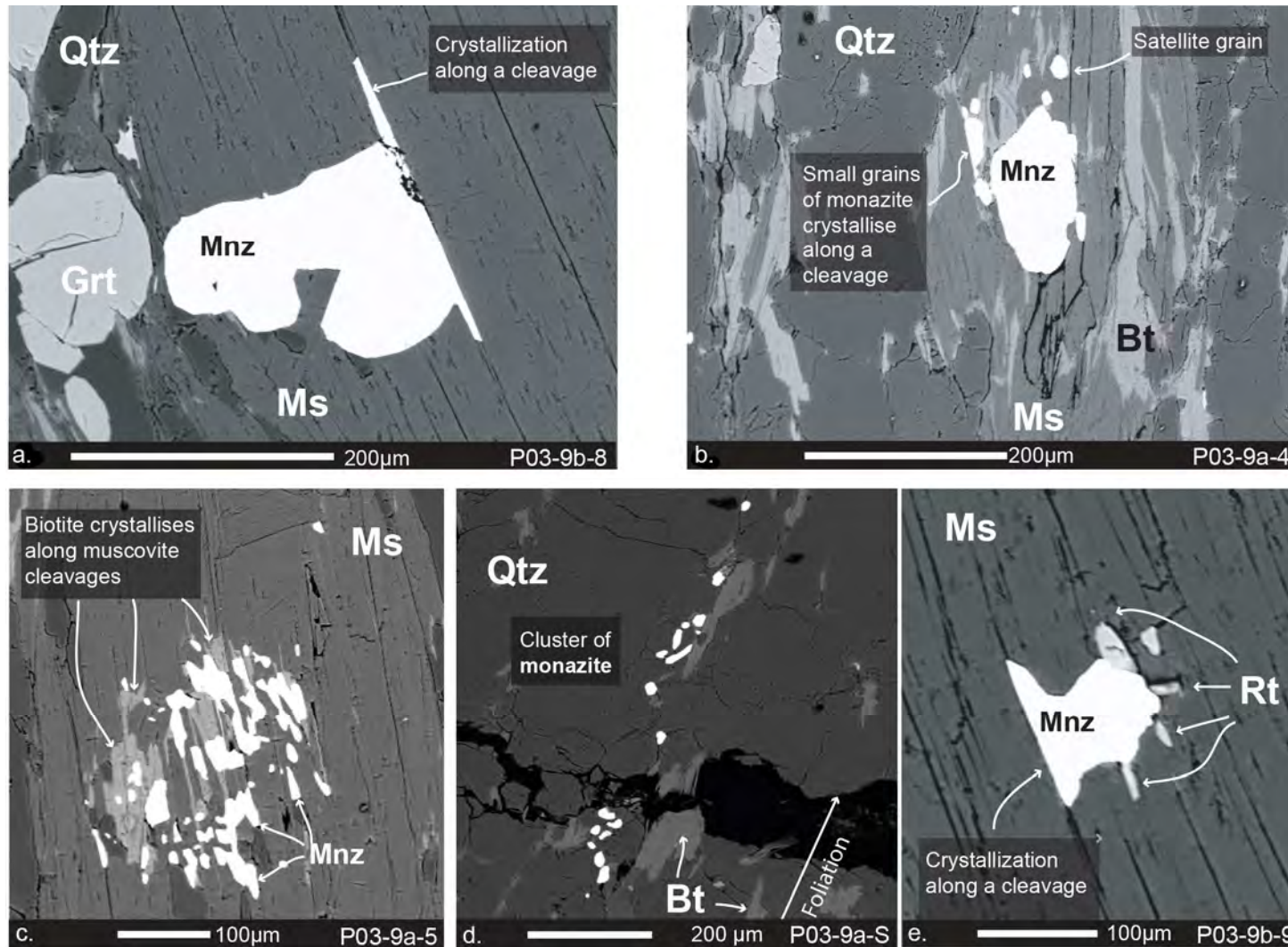




Bosse&Villa - Fig. 3

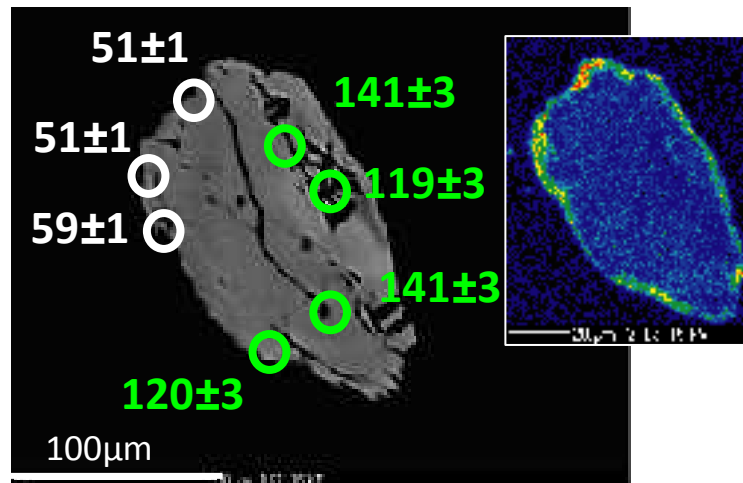
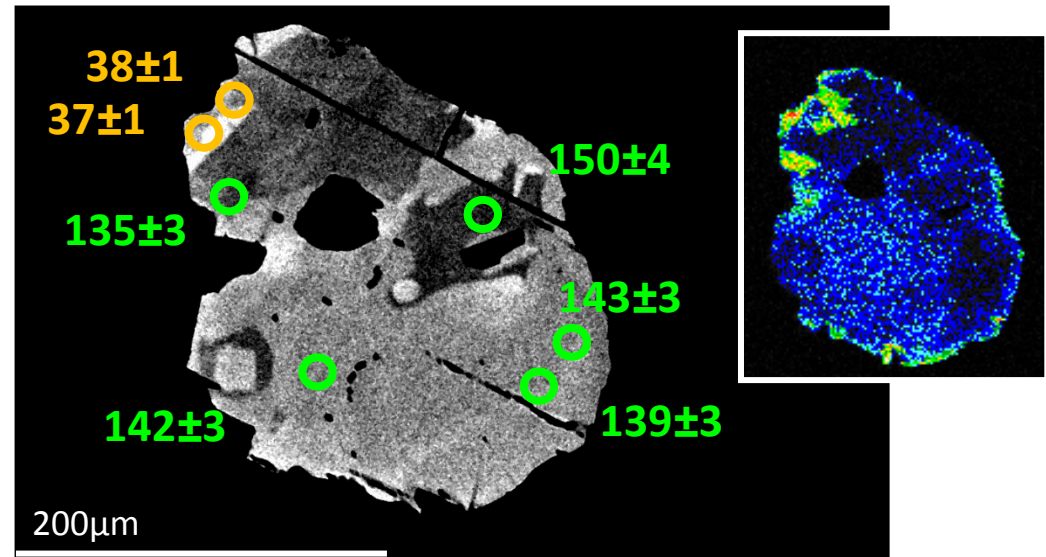
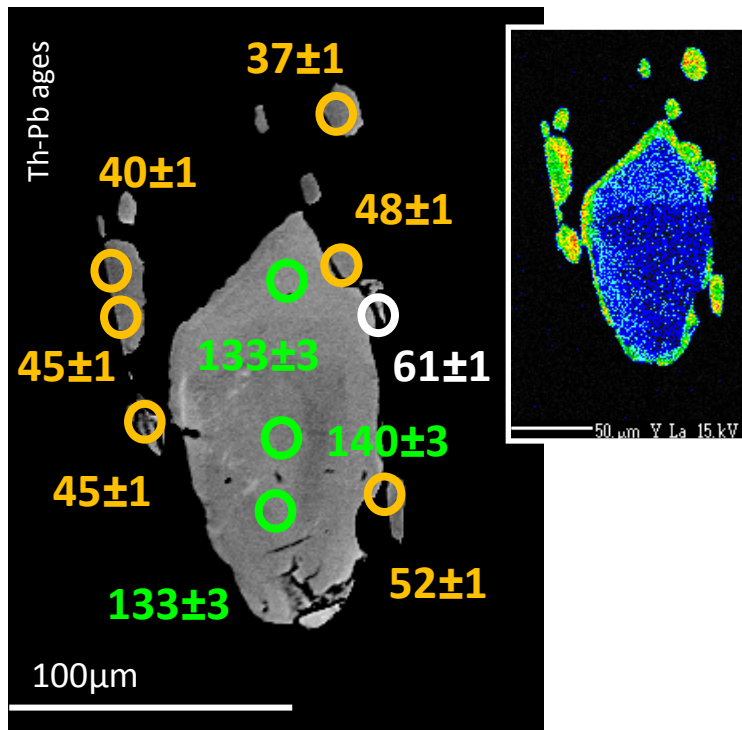


Bosse & Villa - Fig.



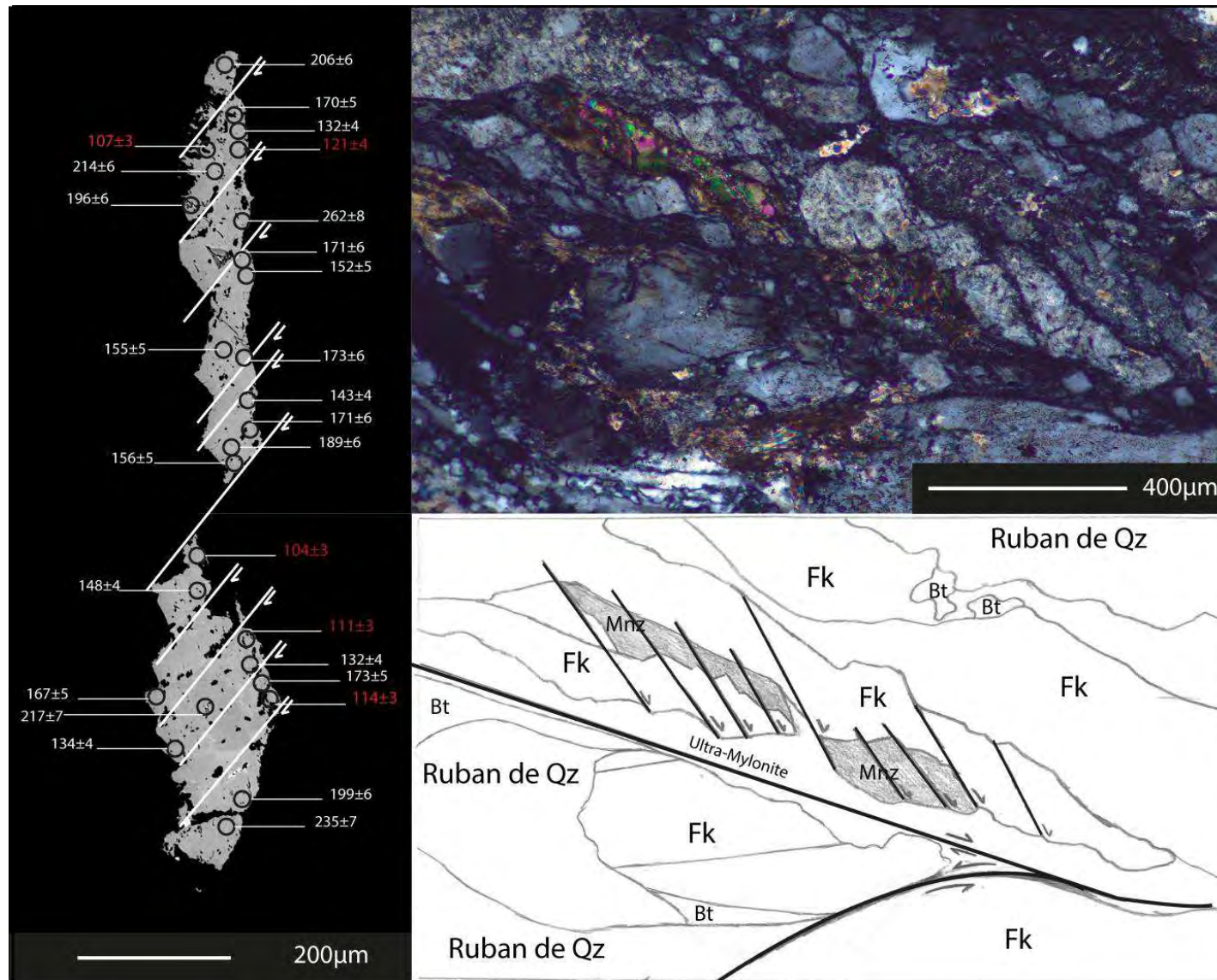
BSE images of monazite from the Rhodope samples (Didier et al. 2014) showing evidences of syn-deformation fluid-assisted monazite growth

Fig. 3



BSE images and Y X-ray maps of matrix monazites in the Rhodope samples (Didier et al. 2014) Circles show the location of the LA-ICPMS pits (11 µm) and their corresponding $^{208}\text{Pb}/^{232}\text{Th}$ ages (2σ level).

Fig. 4



BSE image with $^{232}\text{Th}/^{208}\text{Pb}$ ages (spot size $7\mu\text{m}$). In red, concordant ages and in white mixing (meaningless) ages. Right : Photomicrograph of the monazite texture and sketch showing the deformation.

Fig. 5

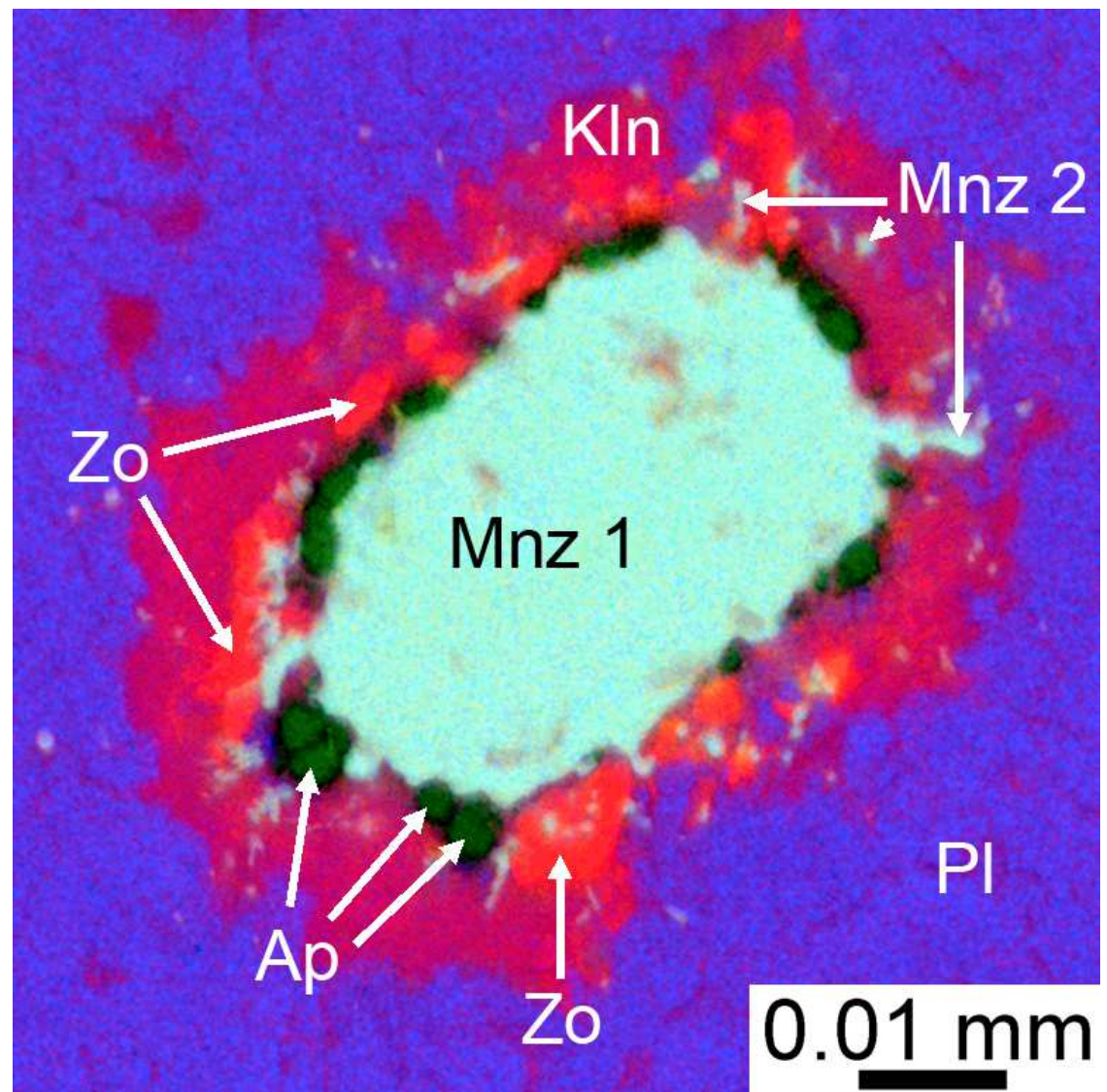
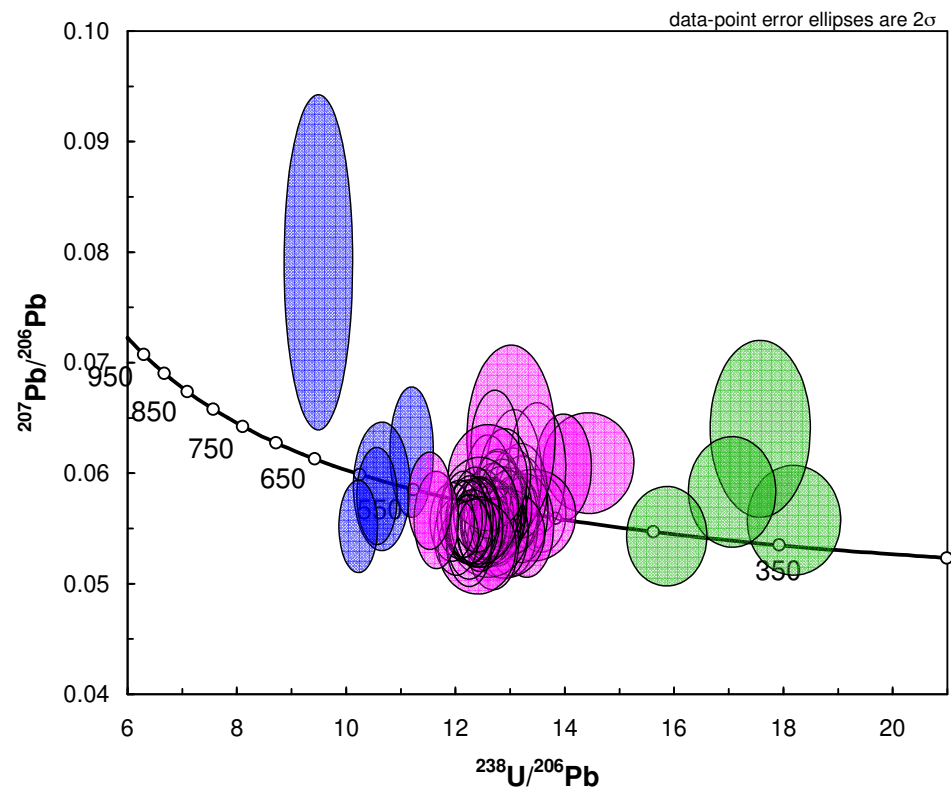


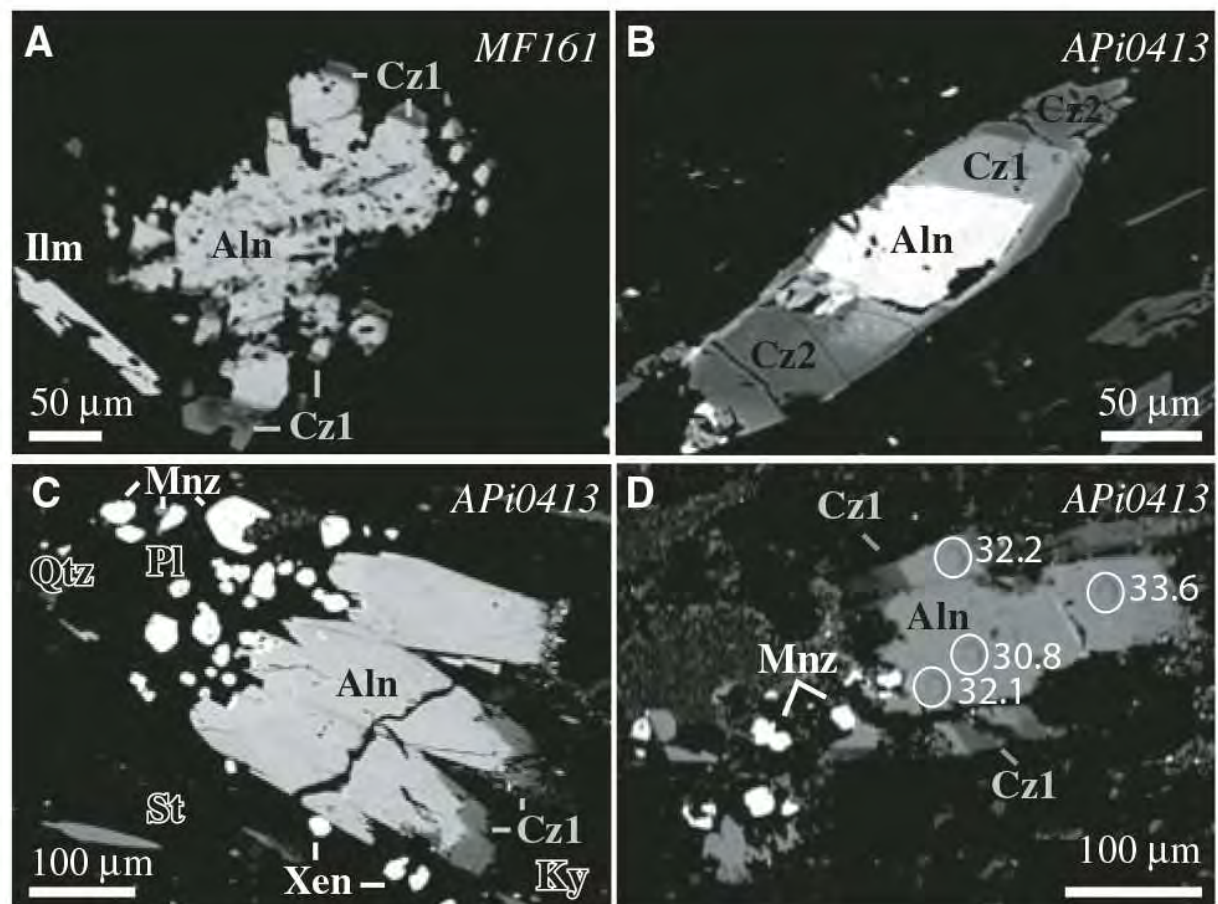
Fig. 6



To be improved ...

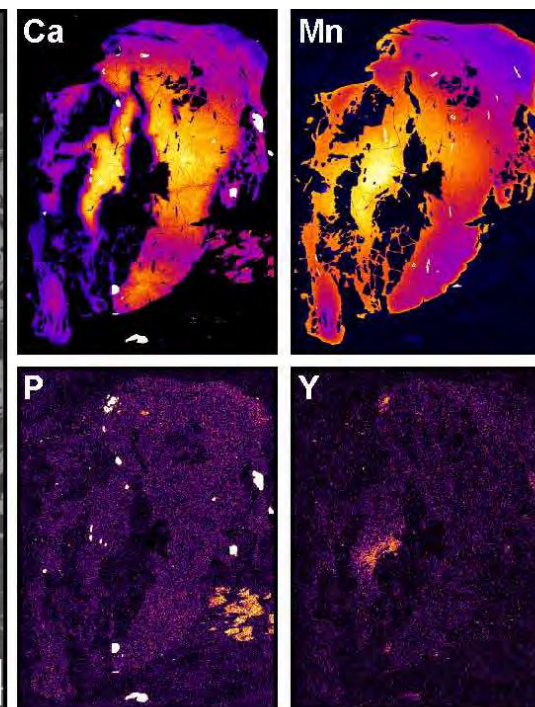
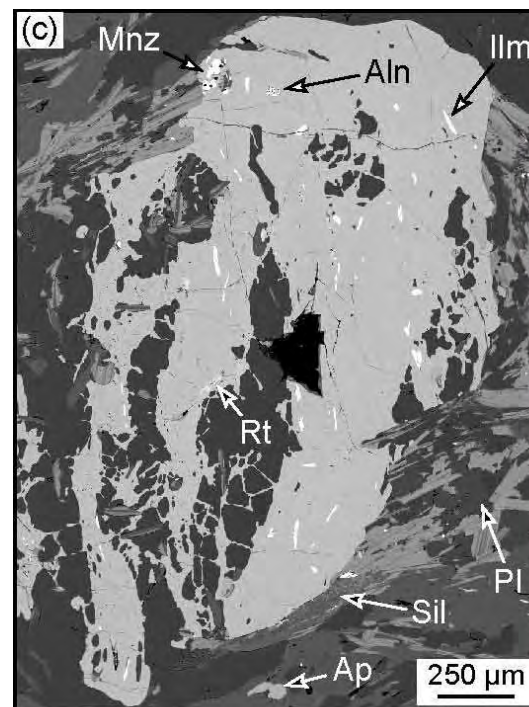
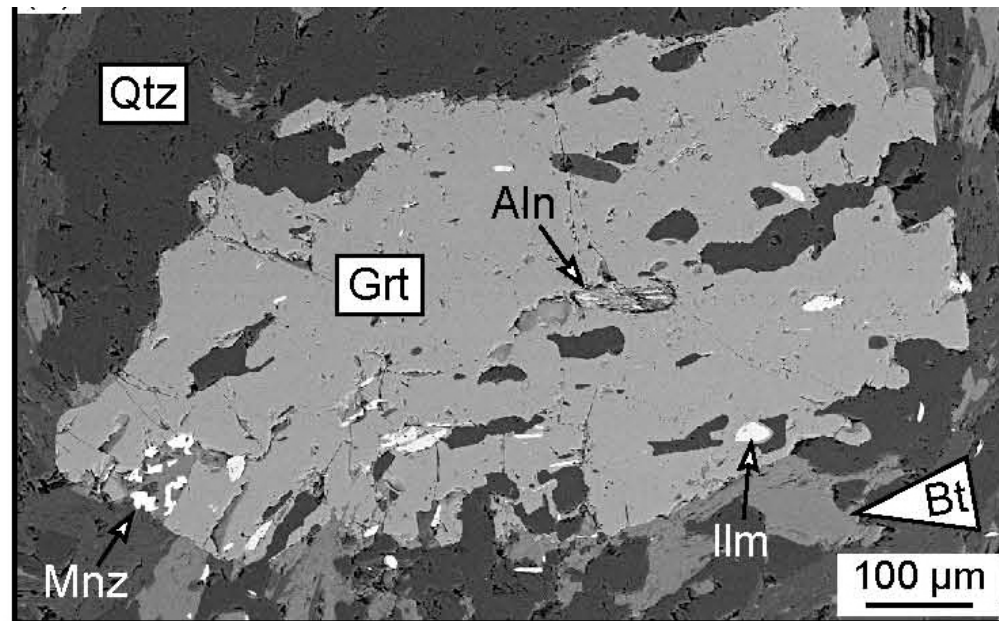
Tera Wasserburg diagram showing the three monazite generations recorded in the Vendée paragneisses (Bosse et al. 2010)

Fig. 7



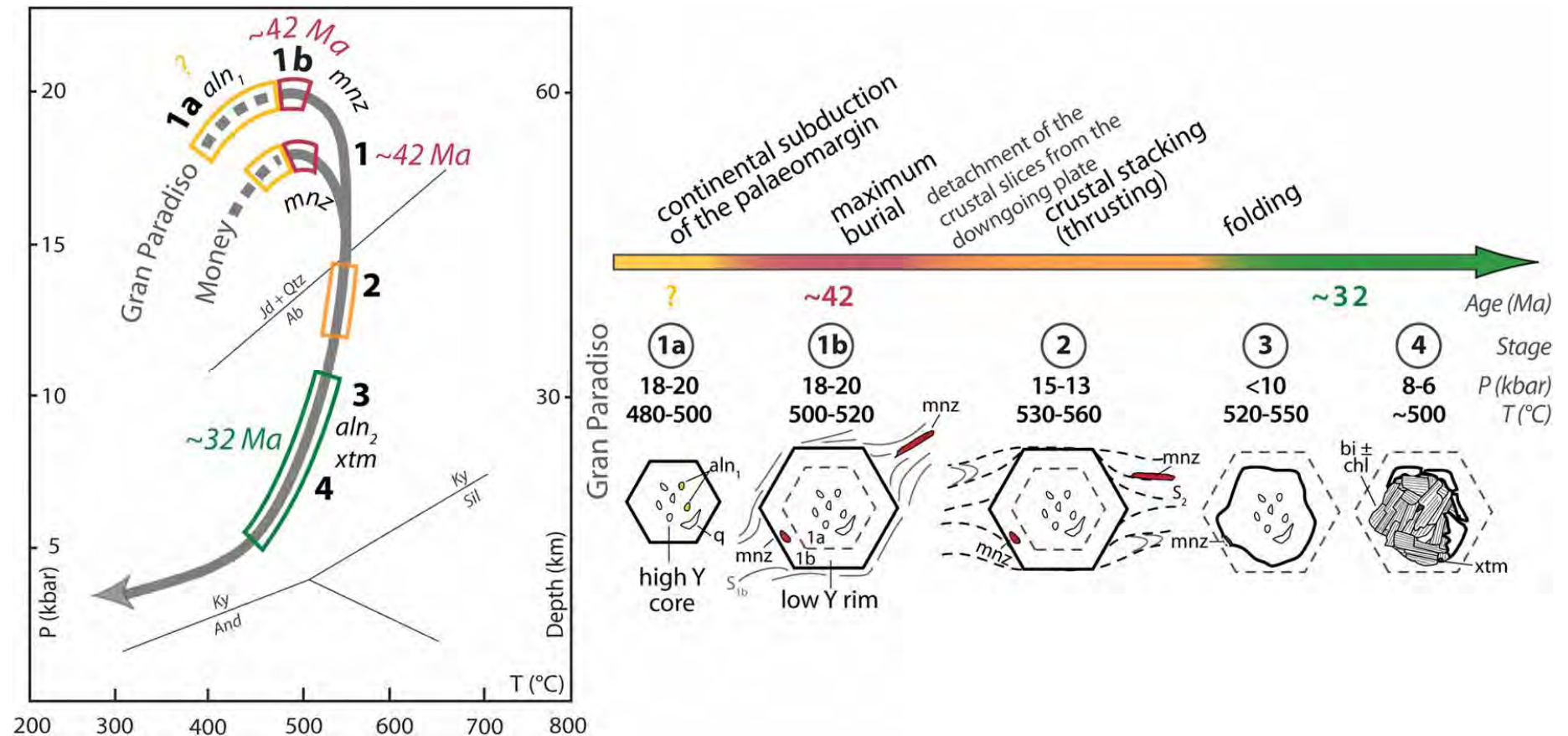
Janots et al. 2009...

Fig. 8



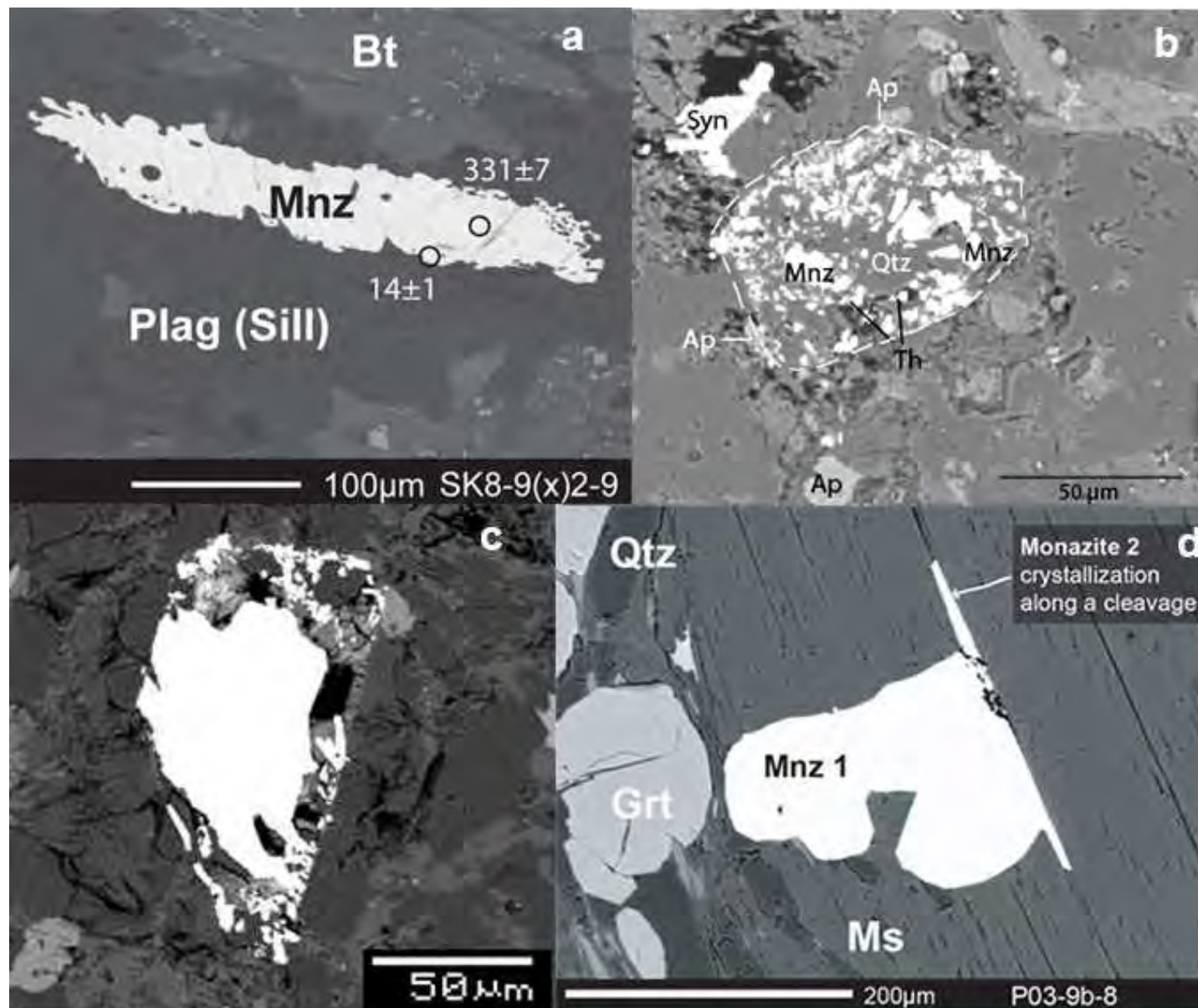
Skrzypek et al. 2016...

Fig. 9



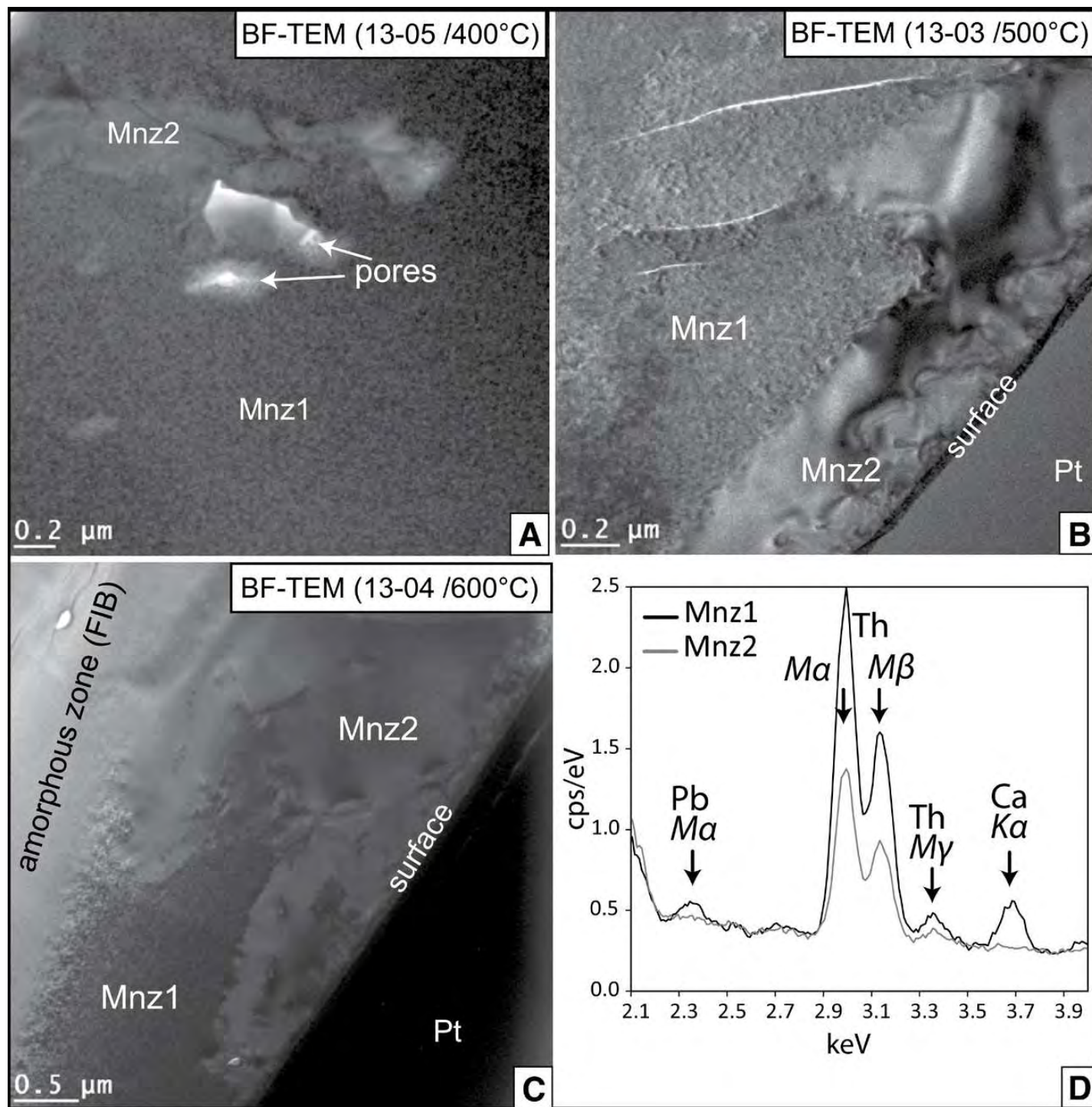
Summary of the petrochronological results (P - T paths and monazite, allanite and xenotime ages) for the Gran Paradiso and Money Units (Manzotti et al. 2018)

Fig. 10



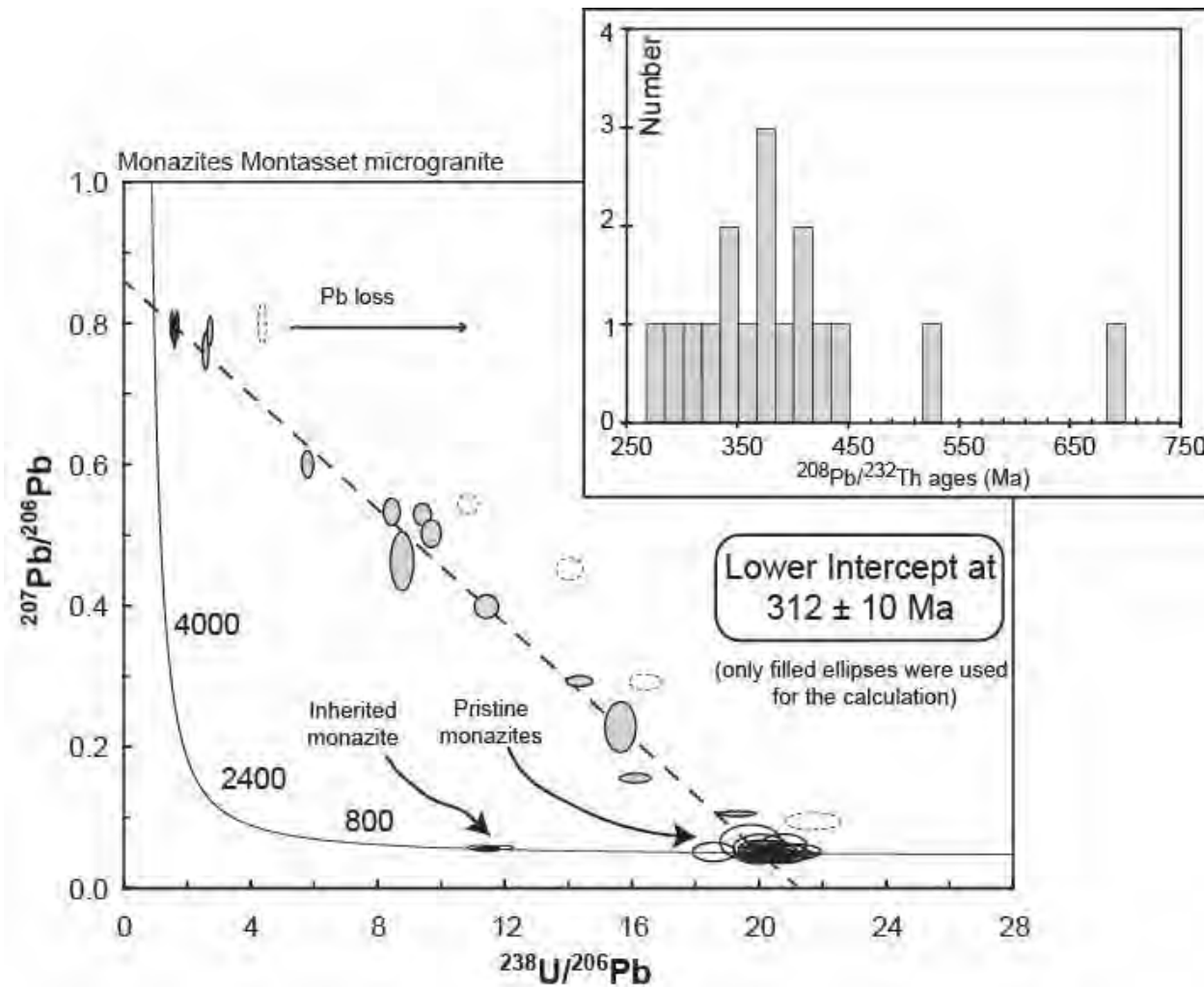
To be modified...

Fig. 11



Grand'Homme et al. 2016

Fig. 12



Tera-Wasserburg diagram of analyses in altered monazites (filled ellipses), in altered monazites affected by Pb loss (dashed ellipses), pristine monazites and an inherited monazite (empty ellipses) from the Montasset microgranite. Only altered monazites (filled ellipses) were used to calculate the U-Pb age at $312 \pm 10 \text{ Ma}$. In the right corner: $^{208}\text{Pb}/^{232}\text{Th}$ age probability histogram for all altered monazites (Didier et al. 2013)